iScience

CellPress
OPEN ACCESS

Article

ILF3 prion-like domain regulates gene expression and fear memory under chronic stress

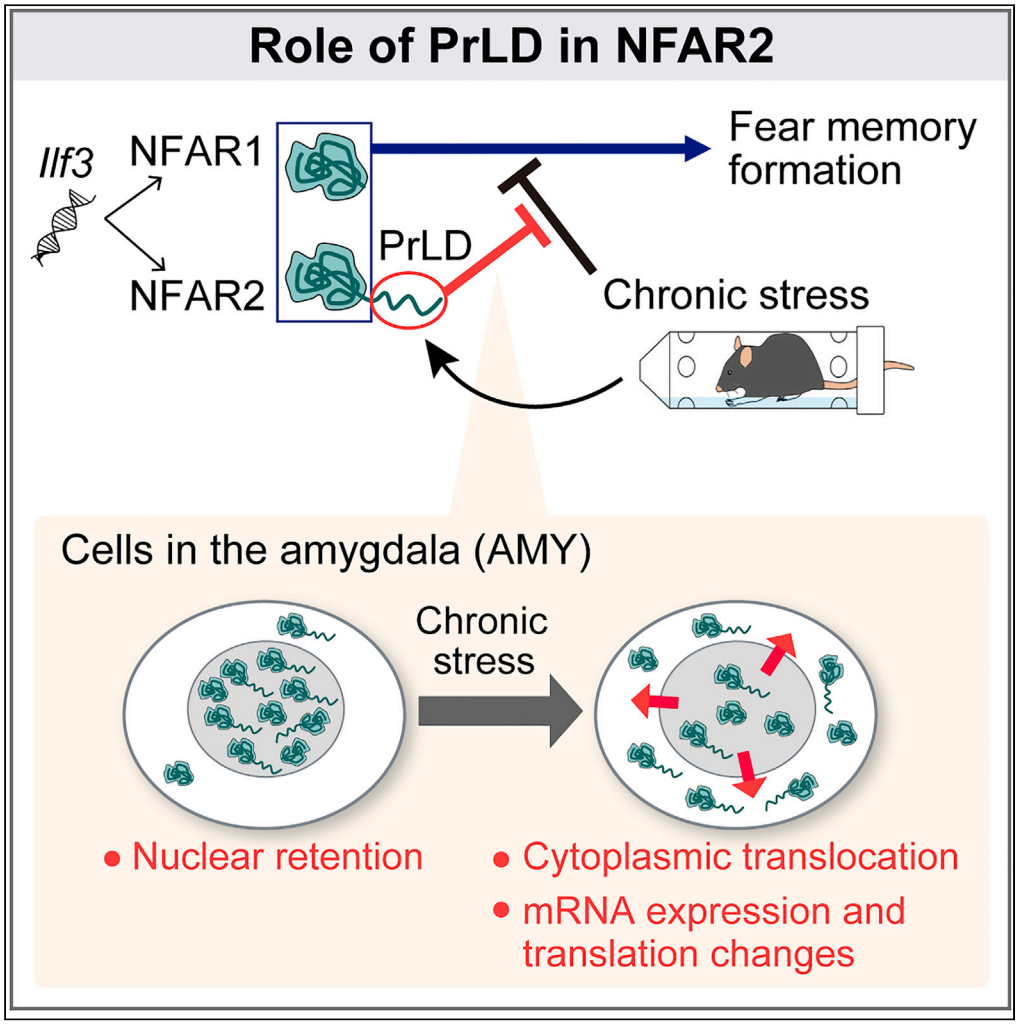

Akira Yamashita, Yuichi Shichino, Kazuki Fujii, ..., Shintaro Iwasaki, Keizo Takao, Nobuyuki Shiina

nshiina@nibb.ac.jp

Highlights

NFAR2 uniquely has a long PrLD, inserted by splicing, among its protein family

PrLD retains NFAR2 in the nucleus in a stress-sensitive manner in AMY

NFAR2 PrLD modifies stress-induced changes in mRNA expression and translation in AMY

NFAR2 PrLD confers chronic stress tolerance in mice in fear memory formation

Yamashita et al., iScience *26*, 106229
March 17, 2023
https://doi.org/10.1016/j.isci.2023.106229

iScience

CellPress
OPEN ACCESS

Article

ILF3 prion-like domain regulates gene expression and fear memory under chronic stress

Akira Yamashita,[1,2] Yuichi Shichino,[3] Kazuki Fujii,[4,5,6] Yumie Koshidaka,[5] Mayumi Adachi,[5] Eri Sasagawa,[7] Mari Mito,[3] Shinichi Nakagawa,[8] Shintaro Iwasaki,[3,9] Keizo Takao,[4,5,6,7] and Nobuyuki Shiina[1,2,10,11,*]

SUMMARY

The prion-like domain (PrLD) is a class of intrinsically disordered regions. Although its propensity to form condensates has been studied in the context of neurodegenerative diseases, the physiological role of PrLD remains unclear. Here, we investigated the role of PrLD in the RNA-binding protein NFAR2, generated by a splicing variant of the *Ilf3* gene. Removal of the PrLD in mice did not impair the function of NFAR2 required for survival, but did affect the responses to chronic water immersion and restraint stress (WIRS). The PrLD was required for WIRS-sensitive nuclear localization of NFAR2 and WIRS-induced changes in mRNA expression and translation in the amygdala, a fear-related brain region. Consistently, the PrLD conferred resistance to WIRS in fear-associated memory formation. Our study provides insights into the PrLD-dependent role of NFAR2 for chronic stress adaptation in the brain.

INTRODUCTION

Intrinsically disordered regions (IDRs) are protein regions that do not form stable three-dimensional structures. IDRs tend to function as hubs for biomolecular complexes by presenting interaction sites with multiple proteins and RNAs.[1,2] Certain IDRs undergo liquid-liquid phase separation (LLPS) to form membraneless organelles (a.k.a. biomolecular condensates) with various proteins and RNAs.[3,4] Through these mechanisms, IDR-containing proteins (IDPs) modulate biochemical reactions positively or negatively, depending on the interaction to other molecules, physical property, and the subcellular localization.[5,6]

A class of IDRs, the prion-like domain (PrLD), has low sequence complexity and is rich in polar amino acids and glycine. This domain has attracted huge attention because its ability to form condensates associated with neurodegenerative diseases, including amyotrophic lateral sclerosis (ALS) and frontotemporal lobar degeneration (FTLD).[7–10] However, most PrLD-containing proteins including fused in sarcoma (FUS), TAR DNA-binding protein-43 (TDP-43), and heterogeneous nuclear ribonucleoprotein A1 (hnRNP A1), whose aggregation causes the diseases listed above, do not form condensates in healthy conditions.[11,12]

Studies in yeasts and plants have suggested that PrLDs diverge in length among orthologs and alternative splicing variants and that the variety confers evolutional advantages in environmental responses and phenotypic diversities.[13–15] In general, the length of IDRs encoded in genome increases with the complexity of the organism.[16,17] Since IDRs are often encoded in alternatively spliced exons,[18,19] the insertion of the IDR may rewire the interaction network of the protein, expanding regulatory layers.[20,21] Although, in vertebrates, the pathological aspects of PrLDs have been well recognized, little is known about the physiological relevance of PrLDs.

Interleukin enhancer-binding factor 3 (*Ilf3*) is a gene conserved in vertebrates and involved in stress responses.[22] Alternative splicing of *Ilf3* generates transcript variants, nuclear factor associated with dsRNA 1 (NFAR1, a.k.a. NF90) and NFAR2 (a.k.a. NF110 and ILF3), the latter of which possesses a PrLD.[23,24] Through the binding to DNA and RNA, both NFAR1 and NFAR2 (NFARs) regulate gene expression in multiple fashions.[25] They are predominantly present in the nucleus to promote and repress transcription, while a fraction of them shuttle between the nucleus and cytoplasm, exporting mRNAs for translation.[26,27] To

[1]Laboratory of Neuronal Cell Biology, National Institute for Basic Biology, Okazaki, Aichi 444-8585, Japan

[2]Department of Basic Biology, The Graduate University for Advanced Studies, SOKENDAI, Okazaki, Aichi 444-8585, Japan

[3]RNA Systems Biochemistry Laboratory, RIKEN Cluster for Pioneering Research, Wako, Saitama 351-0198, Japan

[4]Department of Behavioral Physiology, Faculty of Medicine, University of Toyama, Toyama 930-0194, Japan

[5]Life Science Research Center, University of Toyama, Toyama 930-0194, Japan

[6]Research Center for Idling Brain Science, University of Toyama, Toyama 930-0194, Japan

[7]Department of Behavioral Physiology, Graduate School of Innovative Life Science, University of Toyama, Toyama 930-0194, Japan

[8]RNA Biology Laboratory, Faculty of Pharmaceutical Sciences, Hokkaido University, Sapporo Hokkaido 060-0812, Japan

[9]Department of Computational Biology and Medical Sciences, Graduate School of Frontier Sciences, The University of Tokyo, Kashiwa, Chiba 277-8561, Japan

[10]Exploratory Research Center on Life and Living Systems (ExCELLS), National Institutes of Natural Sciences, Okazaki, Aichi 444-8585, Japan

[11]Lead contact

*Correspondence: nshiina@nibb.ac.jp

https://doi.org/10.1016/j.isci.2023.106229

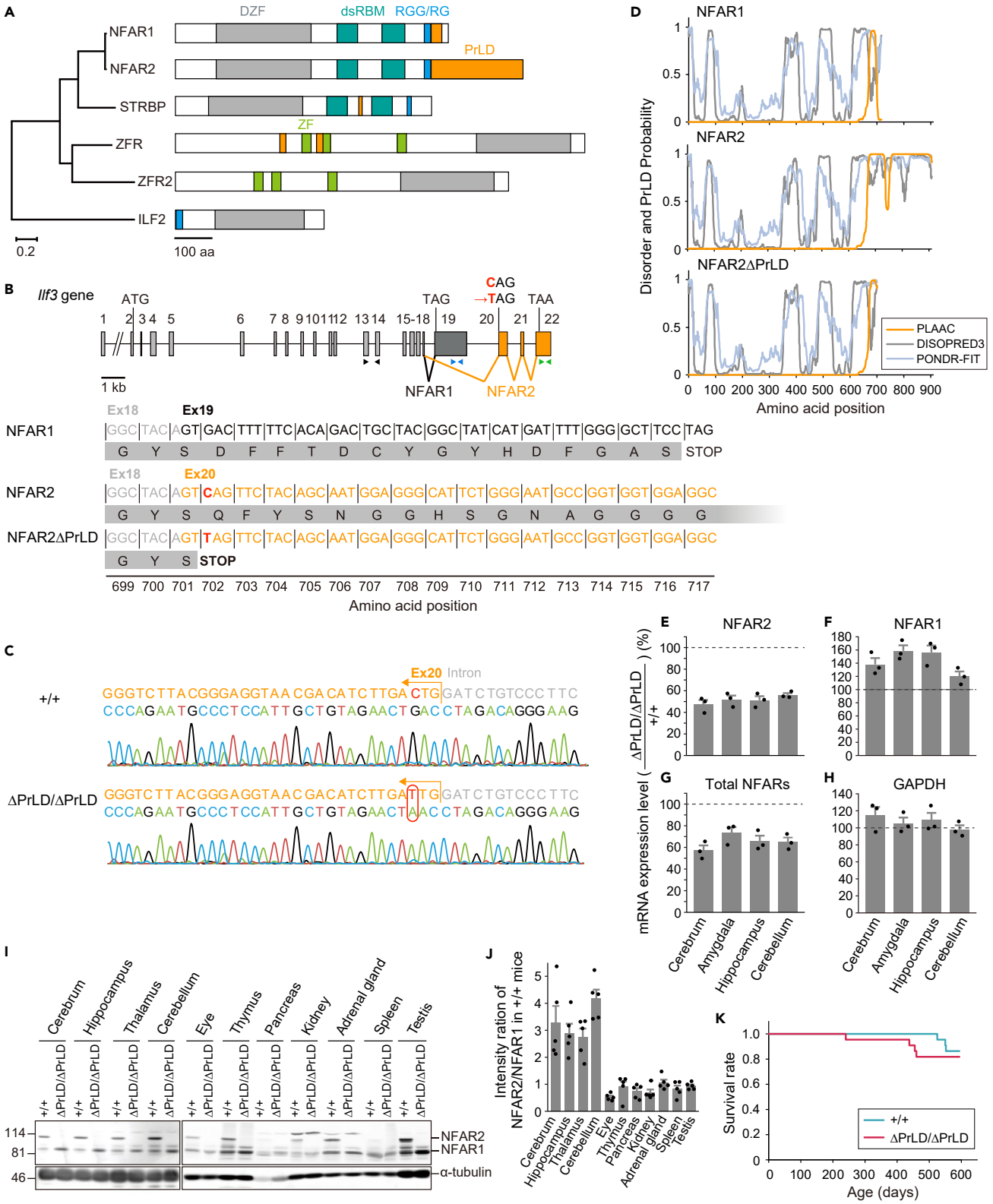
A
DZF
dsRBM
RGG/RG
PrLD
NFAR1
NFAR2
STRBP
ZF
ZFR
ZFR2
ILF2
0.2
100 aa
B
Ilf3 gene
ATG
TAG
CAG
→TAG
TAA
1 kb
NFAR1
NFAR2
Ex18
Ex19
NFAR1
GGC|TAC|AGT|GAC|TTT|TTC|ACA|GAC|TGC|TAC|GGC|TAT|CAT|GAT|TTT|GGG|GCT|TCC|TAG
G Y S D F F T D C Y G Y H D F G A S STOP
Ex18
Ex20
NFAR2
GGC|TAC|AGT|CAG|TTC|TAC|AGC|AAT|GGA|GGG|CAT|TCT|GGG|AAT|GCC|GGT|GGT|GGA|GGC
G Y S Q F Y S N G G H S G N A G G G G
NFAR2ΔPrLD
GGC|TAC|AGT|TAG|TTC|TAC|AGC|AAT|GGA|GGG|CAT|TCT|GGG|AAT|GCC|GGT|GGT|GGA|GGC
G Y S STOP
699 700 701 702 703 704 705 706 707 708 709 710 711 712 713 714 715 716 717
Amino acid position
C
Ex20
Intron
+/+
GGGTCTTACGGGAGGTAACGACATCTTGACTGGATCTGTCCCTTC
CCCAGAATGCCCTCCATTGCTGTAGAACTGACCTAGACAGGGAAG
ΔPrLD/ΔPrLD
GGGTCTTACGGGAGGTAACGACATCTTGATTGGATCTGTCCCTTC
CCCAGAATGCCCTCCATTGCTGTAGAACTAACCTAGACAGGGAAG
D
NFAR1
NFAR2
NFAR2ΔPrLD
Disorder and PrLD Probability
PLAAC
DISOPRED3
PONDR-FIT
0 100 200 300 400 500 600 700 800 900
Amino acid position
E
NFAR2
F
NFAR1
G
Total NFARs
H
GAPDH
mRNA expression level (ΔPrLD/ΔPrLD / +/+) (%)
Cerebrum
Amygdala
Hippocampus
Cerebellum
I
Cerebrum
Hippocampus
Thalamus
Cerebellum
Eye
Thymus
Pancreas
Kidney
Adrenal gland
Spleen
Testis
+/+
ΔPrLD/ΔPrLD
114
81
46
NFAR2
NFAR1
α-tubulin
J
Intensity ration of NFAR2/NFAR1 in +/+ mice
K
Survival rate
+/+
ΔPrLD/ΔPrLD
Age (days)

Figure 1. Generation of *Ilf3*$^{\Delta PrLD/\Delta PrLD}$ mice

(A) Phylogenetic tree of DZF-containing proteins in mice. DZF, double zinc-finger domain; dsRBM, dsRNA-binding motif; RGG/RG, Arg-Gly-Gly/Arg-Gly motif; ZF, C2H2-type zinc-finger domain; PrLD, prion-like domain predicted by PLAAC. Scale bars indicate the number of amino acid substitutions per site (left) and the number of amino acids (right).

(B) Alternative splicing pattern of the mouse *Ilf3* gene. The nucleotide and amino acid sequences of NFAR1, NFAR2, and NFAR2ΔPrLD near the splice junction of exon 18 terminal are shown. In NFAR2ΔPrLD, a single nucleotide substitution from C to T (red) introduced a stop codon at the beginning of exon 20. The positions of the primers used for quantitative RT-PCR in E-G are indicated by triangles: black, NFARs; blue, NFAR1; green, NFAR2.

(C) Representative DNA sequencing in mouse genotyping. For simplicity, *Ilf3*$^{+/+}$ and *Ilf3*$^{\Delta PrLD/\Delta PrLD}$ are denoted as +/+ and ΔPrLD/ΔPrLD, respectively. The antisense strand was sequenced. A red circle indicates the C to T substitution.

(D) IDR and PrLD prediction by DISOPRED3 and PONDR-FIT for IDR and by PLAAC for PrLD.

(E–H) Relative expression levels of mRNAs in the brain of *Ilf3*$^{\Delta PrLD/\Delta PrLD}$ mice compared with *Ilf3*$^{+/+}$ mice. GAPDH is a control. Data are represented as the mean ± SEM with dot plots of individual values. n = 3.

(I) Western blotting of tissues from the *Ilf3*$^{+/+}$ and *Ilf3*$^{\Delta PrLD/\Delta PrLD}$ mice for NFARs and α-tubulin as a control.

(J) Intensity ratio of NFAR2/NFAR1 in the tissues of *Ilf3*$^{+/+}$ mice in Western blotting. n = 5, $p < 0.0001$, one-way ANOVA.

(K) Survival curves of *Ilf3*$^{+/+}$ and *Ilf3*$^{\Delta PrLD/\Delta PrLD}$ mice. n = 22, p = 0.6, log rank test.

See also Figure S1.

respond to virus infection and oxidative stress, NFARs suppress or facilitate translation depending on target mRNAs.[22,28,29]

In contrast to these common functions, NFAR1 and NFAR2 differ in subcellular and subnuclear localization. NFAR2 is more prone to be in the nucleus than NFAR1, due to the PrLD.[26] Within the nucleus, both NFAR1 and NFAR2 are localized in the nucleolus in common, while only NFAR2 is also enriched in the nucleoplasm.[25,30,31] In the cytoplasm, NFAR2, but not NFAR1, localizes to the RNP condensate formed by RNG105 (a.k.a. caprin1), a component of neuronal RNA granules and stress granules.[32] Given that the potential functional difference of subcellular localization originates from PrLD, further phenotypic studies of NFARs mutants will provide a better understanding of the physiological implications of PrLDs.

For that purpose, we generated *Ilf3* mutant mice by deleting the PrLD in NFAR2 (*Ilf3*$^{\Delta PrLD/\Delta PrLD}$ mice). In addition, since NFARs have stress-responsive functions, we applied chronic stress to mice, which is known to increase oxidative stress levels in the brain.[33,34] Through the investigations by microscopic analysis, ribosome profiling, and behavioral tests, we found that the PrLD of NFAR2 mediates the nuclear retention, regulates chronic stress-dependent changes in mRNA expression and translation, and enables mice to better form conditioned fear memory in a chronic stress environment. These results suggest that the PrLD confers versatility for responding to the environment, by subcellular localization modulation rather than condensate formation.

RESULTS

Prion-like domain insertion in domain associated with zinc finger family proteins

NFARs belong to a metazoan-exclusive protein family containing the domain associated with zinc fingers (DZF domain). This family consists of interleukin enhancer-binding factor 2 (ILF2), zinc-finger protein associated with RNA (ZFR), ZFR2, spermatid perinuclear RNA-binding protein (SPNR, a.k.a. STRBP), and ILF3 (NFARs) (Figure 1A). Of these proteins, ZFR2, STRBP, and NFARs are uniquely found in vertebrates (Figure S1). Among these paralogs, only NFAR2 has a long PrLD (over 200 amino acids) (Figures 1A and S1). Although medium-length PrLDs (100-200 amino acids) are present also in ZFR2 in fish and reptiles, the corresponding region of mammalian ZFR2 is replaced with non-PrLD type IDR (Figure S1). These suggest that the insertion of PrLDs occurred in selective proteins and species. Notably, despite the absence of long PrLDs, STRBP, a closely related paralog of NFARs, plays an important role in brain and sperm function[35] as NFARs do. The paralog-wise and isoform-wise comparison led us to study the roles of the uniquely long PrLD in NFAR2.

Generation of *Ilf3*$^{\Delta PrLD/\Delta PrLD}$ mice that lack the prion-like domain of NFAR2

To investigate the physiological roles of the PrLD in NFAR2, we deleted the domain in mice (*Ilf3*$^{\Delta PrLD/\Delta PrLD}$ mice). Compared to NFAR1, NFAR2 contains more exons at the 3′ end, skipping exon 19 and obtaining exons 20-22 (Figure 1B), and yields NFAR2-specific amino acid residues (702-911) (Figure 1B). The 702-911 region was predicted as IDR[32] and as a part of PrLD (671-911) (Figure 1D). In contrast, NFAR1 possesses a short trait of the predicted PrLD (671-698). Given that, we designed to introduce a stop codon at the 5′ end of exon 20, to delete the PrLD from NFAR2. The replacement of c.2104C to T with CRISPR/Cas9

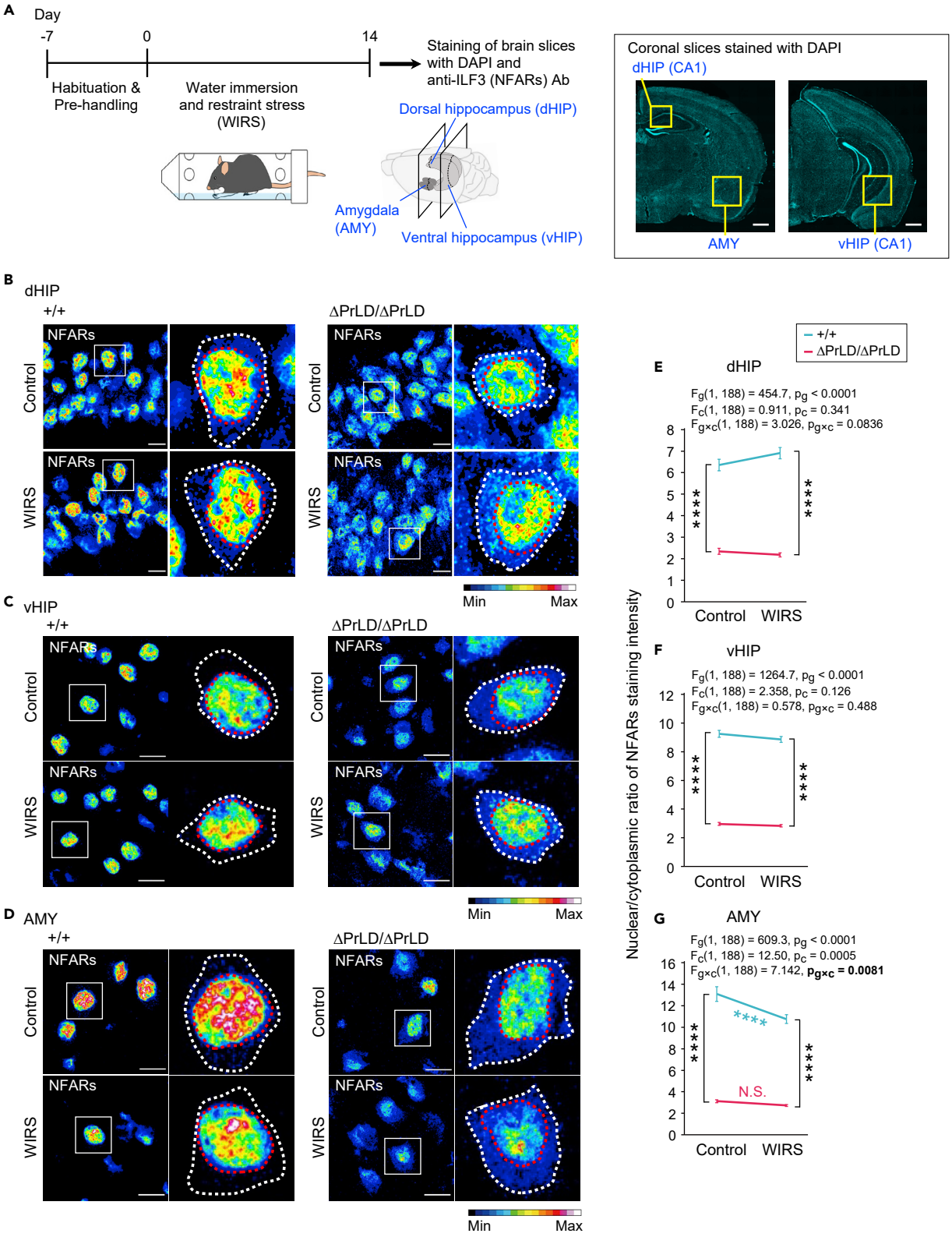
A
Day
-7
0
14
Staining of brain slices with DAPI and anti-ILF3 (NFARs) Ab
Habituation & Pre-handling
Water immersion and restraint stress (WIRS)
Dorsal hippocampus (dHIP)
Amygdala (AMY)
Ventral hippocampus (vHIP)
Coronal slices stained with DAPI
dHIP (CA1)
AMY
vHIP (CA1)
B
dHIP
+/+
ΔPrLD/ΔPrLD
NFARs
Control
WIRS
Min
Max
C
vHIP
D
AMY
E
dHIP
+/+
ΔPrLD/ΔPrLD
Fg(1, 188) = 454.7, pg < 0.0001
Fc(1, 188) = 0.911, pc = 0.341
Fg×c(1, 188) = 3.026, pg×c = 0.0836
F
vHIP
Fg(1, 188) = 1264.7, pg < 0.0001
Fc(1, 188) = 2.358, pc = 0.126
Fg×c(1, 188) = 0.578, pg×c = 0.488
G
AMY
Fg(1, 188) = 609.3, pg < 0.0001
Fc(1, 188) = 12.50, pc = 0.0005
Fg×c(1, 188) = 7.142, pg×c = 0.0081
****
N.S.
Nuclear/cytoplasmic ratio of NFARs staining intensity
Control
WIRS

Figure 2. PrLD deletion reduces nuclear retention of NFARs and attenuates amygdala-specific sensitivity of the nuclear retention to chronic stress WIRS

(A) Schematic of NFARs subcellular localization analysis after WIRS. The right panels are DAPI staining of brain slices showing the brain regions. Scale bars, 1 mm.

(B–D) Representative heatmap images of NFARs stained in the dHIP (B), vHIP (C), and AMY (D) of *Ilf3*$^{+/+}$ and *Ilf3*$^{\Delta PrLD/\Delta PrLD}$ mice. In the right magnified images, the white and red dotted lines outline the cells and nuclei, respectively. Scale bars, 10 μm.

(E–G) Nuclear-cytoplasmic ratio of NFARs staining intensity in the brain regions. The data are presented as mean ± SEM. n = 48 pictures from three mice in each group. The data were analyzed using two-way ANOVA. The F-values and p values for the main effects of the genotypes (F_g and p_g, respectively), conditions (with or without WIRS) (F_c and p_c, respectively), and interactions between the genotypes and conditions ($F_{g\times c}$ and $p_{g\times c}$, respectively) are indicated. In E and F, ****$p < 0.0001$ in Tukey-Kramer test after the two-way ANOVA. In G, ****$p < 0.0001$ in simple effect analysis after significant interaction in the two-way ANOVA. N.S., no significant difference ($p \geq 0.05$).

See also Figures S2 and S3.

resulted in the truncated NFAR2 (amino acid residues 1-701) (Figures 1B–1D). Since the mutated NFAR2 mRNA has the premature stop codon, it was expected to be degraded by a nonsense-mediated decay (NMD) pathway.[36] Consistent with this scenario, NFAR2 mRNA partially reduced in *Ilf3*$^{\Delta PrLD/\Delta PrLD}$ mice compared with wild-type (*Ilf3*$^{+/+}$) mice (Figure 1E).

However, the remained mRNA may lead to NFAR2ΔPrLD protein translation. Western blotting of mouse tissues with ILF3 antibody detected two proteins in different sizes at 90 kDa and 110 kDa, corresponding to NFAR1 and NFAR2, respectively. The 110 kDa protein disappeared in all tissues from the *Ilf3*$^{\Delta PrLD/\Delta PrLD}$ mice (Figure 1I). In contrast, the intensity of the 90 kDa protein was increased 1- to 2-fold in most tissues from the *Ilf3*$^{\Delta PrLD/\Delta PrLD}$ mice. This may be due to the similar migration of NFAR2ΔPrLD and NFAR1 on SDS-PAGE and partially due to an increased NFAR1 mRNA (Figure 1F) for unknown reasons.

While *Ilf3* knockout mice are perinatal lethal because of neuromuscular respiratory failure,[37] the *Ilf3*$^{\Delta PrLD/\Delta PrLD}$ mice were viable without a significant decrease in their survival rate (Figure 1K). However, the effect of PrLD deletion could be more prevailing in tissues such as the brain, where NFAR2 expression predominates over NFAR1 (Figure 1J). Therefore, we investigated the effects of PrLD deletion in the brain on the subcellular localization of NFARs, mRNA expression and translational regulation, and mouse behavior, across chronic stress.

Prion-like domain of NFAR2 is responsible for the chronic stress-sensitive nuclear retention in the amygdala

First, we immunostained NFARs in the brain (Figure 2A). NFARs were predominantly localized in the nucleus of brain regions including the dorsal hippocampus (dHIP), ventral HIP (vHIP), and amygdala (AMY) in the *Ilf3*$^{+/+}$ mice (Figures 2B–2D). Although NFARs diffused in the nucleoplasm, a part of them accumulated in nuclear condensates (granules), as previously reported[38] (Figure S2A). The *Ilf3*$^{\Delta PrLD/\Delta PrLD}$ mice reduced NFARs in the nucleoplasm (Figure S2A) and tended to reduce the nuclear granule formation (Figures S2B–S2L), resulting in the declined nuclear-cytoplasmic ratio of NFARs (Figures 2B–2G). These results suggested that PrLD-deficient forms (NFAR1 and NFAR2ΔPrLD) have a weaker ability to localize in the nucleus. This reduction was primarily due to the loss of NFARs from the nucleoplasm, which is consistent with previous reports that PrLD-containing NFAR2 is more abundant in the nucleoplasm than NFAR1.[25,30]

Next, we stressed those brain regions and tested the localization alteration of NFARs. For this purpose, we harnessed chronic water immersion and restraint stress (WIRS) in mice (Figure 2A), which causes oxidative damage to the most stress-sensitive AMY and HIP in the brain.[33,34] Mice were subjected to 3 h WIRS daily for 14 days. This treatment resulted in weight loss in the mice, a hallmark of chronic stress (Figure S11A). Although the impacts on NFARs in the dHIP and vHIP were limited, WIRS reduced the nuclear-cytoplasmic ratio in the AMY of *Ilf3*$^{+/+}$ mice (Figures 2B–2G). This WIRS-induced decrease originated from the loss of the diffuse staining in the nucleoplasm, without associated decreases in the number or size of the nuclear granules (Figures S2K and S2L). Remarkably, the *Ilf3*$^{\Delta PrLD/\Delta PrLD}$ mice lost this response to WIRS in the AMY (Figures 2D and 2G), whereas no effect in the dHIP or vHIP was observed as in the wild type (Figures 2B, 2C, 2E, and 2F). This phenotype could be attributed to the low nucleoplasm localization of NFARs in *Ilf3*$^{\Delta PrLD/\Delta PrLD}$ mice even without stress (Figure S2F). Taken together, these results suggested that the PrLD of NFAR2 is responsible for the nucleoplasmic retention of NFARs, which is sensitive to chronic stress in the AMY.

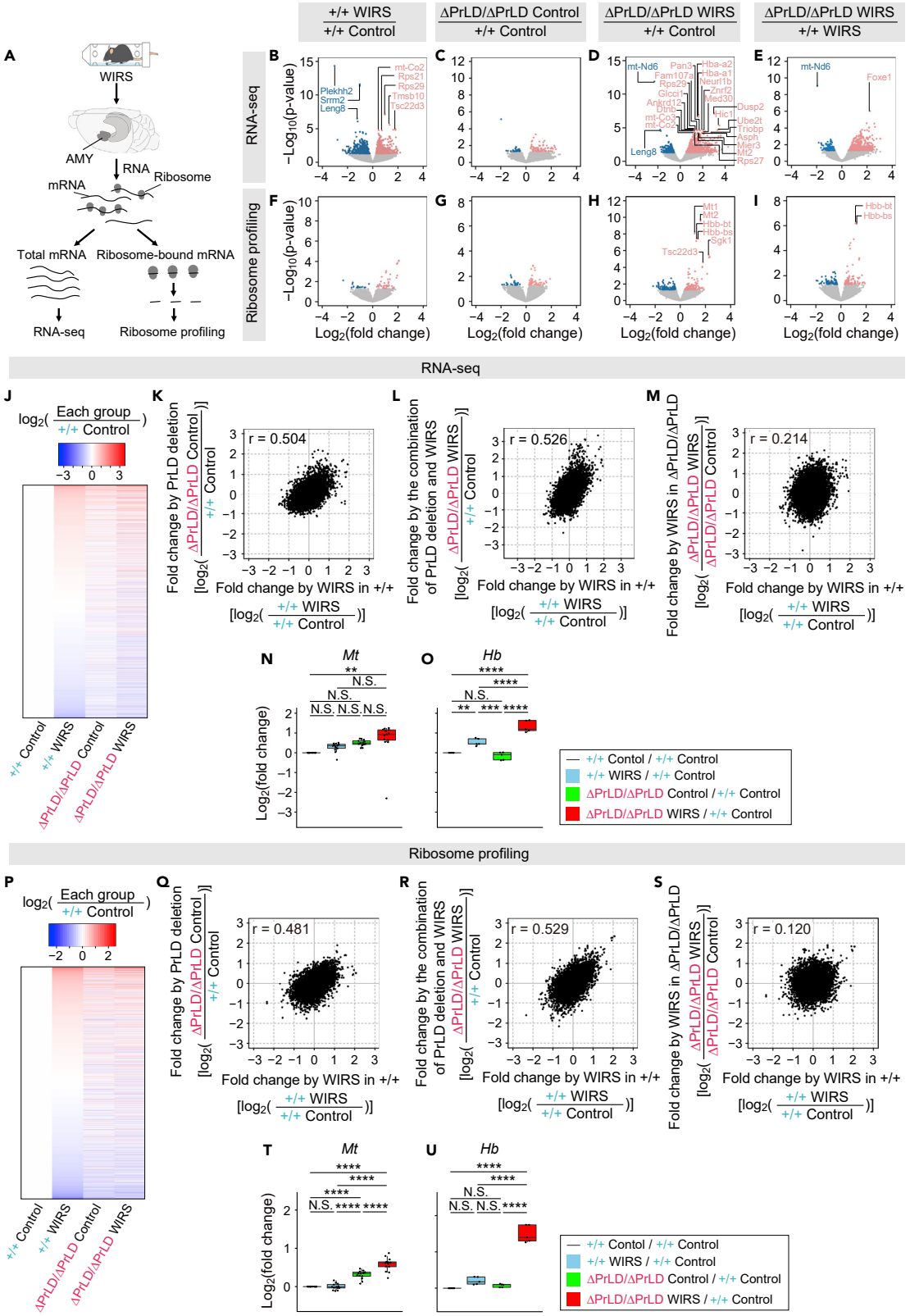
+/+ WIRS / +/+ Control
ΔPrLD/ΔPrLD Control / +/+ Control
ΔPrLD/ΔPrLD WIRS / +/+ Control
WIRS
AMY
RNA
mRNA
Ribosome
Total mRNA
Ribosome-bound mRNA
RNA-seq
Ribosome profiling
RNA-seq
Ribosome profiling
r = 0.504
r = 0.526
r = 0.214
r = 0.481
r = 0.529
r = 0.120
Mt
Hb
+/+ Contol / +/+ Control
+/+ WIRS / +/+ Control
ΔPrLD/ΔPrLD Control / +/+ Control
ΔPrLD/ΔPrLD WIRS / +/+ Control

Figure 3. PrLD deletion-caused and WIRS-induced changes in mRNA expression and translation in the AMY

(A) Schematic of RNA-seq and ribosome profiling in the AMY.

(B–I) Volcano plots of differential mRNA expression (B–E) and differential translation (F–I). WIRS-induced changes in the *Ilf3*$^{+/+}$ mice (B and F), PrLD deletion-caused changes under control conditions (C and G), changes by the combinational effects of PrLD deletion and WIRS (D and H), and PrLD deletion-caused changes under WIRS (E and I). Blue and red dots indicate transcripts with $p < 0.05$. The names of transcripts with $q < 0.05$ are shown.

(J) Heatmap showing the fold changes in mRNA expression by WIRS, PrLD deletion, and the combinational effects of PrLD deletion and WIRS.

(K–M) Scatterplots and Pearson correlation coefficients (r) comparing changes in mRNA expression. WIRS-induced changes in the *Ilf3*$^{+/+}$ mice were compared with the changes caused by PrLD deletion (K); with the changes caused by the combinational effects of PrLD deletion and WIRS (L); and with WIRS-induced changes in the *Ilf3*$^{\Delta PrLD/\Delta PrLD}$ mice (M).

(N and O) Boxplots showing the changes in mRNA expression of the mitochondrial genome-encoded genes (*Mt*) (N) and the hemoglobin genes (*Hb*) (O).

(P) Heatmap showing the fold changes in translation by WIRS, PrLD deletion, and the combinational effects of PrLD deletion and WIRS. Note that the order of transcripts is different from that in J.

(Q–S) Scatterplots and Pearson correlation coefficients (r) comparing changes in translation. The horizontal and vertical axes are the same as in K–M.

(T and U) Boxplots showing the changes in the translation of the *Mt* (T) and *Hb* (U) genes.

****$p < 0.0001$, ***$p < 0.001$, **$p < 0.01$, Welch's t-test with Bonferroni correction. N.S., no significant difference ($p \geq 0.05$).

See also Figure S4 and Tables S1, S2, S3, S4, S5, S6, S7, S8, and S9.

We also tested the effect of WIRS on the nuclear-cytoplasmic localization of other PrLD-bearing proteins TDP-43 and hnRNP A1 in the AMY. In contrast to NFARs, their localizations were largely unchanged by WIRS (Figures S3A–S3D). TDP-43 and hnRNP A1 have been reported to translocate from the nucleus to the cytoplasm upon osmotic stress, but much less translocation induced by oxidative stress.[39,40] Thus, PrLD-containing proteins commonly display stress-sensitive nuclear retention, but the type and intensity of stress that induces translocation to the cytoplasm may differ among them.

Deletion of NFAR2 prion-like domain alters water immersion and restraint stress-induced changes in mRNA expression and translation in the amygdala

Since NFARs have been reported to participate in gene expression controls in a stress-dependent manner, we explored the role of the PrLD in mRNA expression by RNA-seq in the AMY (Figure 3A). First, we investigated the WIRS-induced mRNA expression changes in *Ilf3*$^{+/+}$ mice (Figure 3B; Table S1A). Indeed, our data recapitulated the stress-inducible gene expression reported in earlier studies: glucocorticoid-inducible factor *Tsc22d3* mRNA, whose transcriptional activation was reported upon psychological stress,[41] and serum and glucocorticoid-regulated kinase 1 (*Sgk1*), which is known as the gene upregulated by WIRS[42] (Figures 3B and S4Q; Table S1A). More broadly, Gene ontology (GO) enrichment analysis revealed that the overrepresented GO terms for up-regulated genes consisted of "Ribosome," "Nucleosome assembly," "Oxidative phosphorylation," and "Parkinson disease" (Figure S4A; Table S2A). These GO terms associated with the ribosome and mitochondrial functions were consistent with the previous study in the prefrontal cortex of chronically stressed mice.[43] These data ensured the chronic stress induction by WIRS in our experimental conditions.

Next, the effects of PrLD deletion on mRNA expression were analyzed (Figure 3C; Table S1B). We noticed that *Ilf3*$^{\Delta PrLD/\Delta PrLD}$ mice showed a stress-like gene expression pattern even without WIRS: mRNA expression profile in *Ilf3*$^{\Delta PrLD/\Delta PrLD}$ mice was highly correlated with that in the WIRS-treated *Ilf3*$^{+/+}$ mice (Figures 3J and 3K; Table S5A). As observed in WIRS-induced mRNA changes in *Ilf3*$^{+/+}$ mice (Figure S4A; Table S2A), similar GO terms (such as "Oxidative phosphorylation" and "Parkinson disease") were also found in mRNAs overexpressed in *Ilf3*$^{\Delta PrLD/\Delta PrLD}$ mice (Figure S4B; Table S2B). Thus, NFAR2 PrLD deletion shifted the transcriptome profile to that reminiscent of chronic stress conditions.

WIRS treatment of the PrLD-deficient mice still maintained the stress-related gene induction or even enhanced it (Figures 3D and 3E; Tables S1C and S1D). Overall mRNA expression in the WIRS-treated *Ilf3*$^{\Delta PrLD/\Delta PrLD}$ mice was congruent with that in the *Ilf3*$^{+/+}$ mice with WIRS (Figures 3J, 3L, and S4C; Tables S2C and S5A). Specifically, WIRS-responsive mRNAs (defined as genes up-regulated in mRNA abundance by WIRS in *Ilf3*$^{+/+}$ mice, Figure 3B, red dots) were also upregulated in WIRS-treated *Ilf3*$^{\Delta PrLD/\Delta PrLD}$ mice (Figure S4G; Table S7A). Also, mitochondrial genome-encoded genes (*Mt*) and hemoglobin genes (*Hb*), whose expressions are considered to be markers of chronic stress in the mouse brain,[43–45] were upregulated rather more in *Ilf3*$^{\Delta PrLD/\Delta PrLD}$ mice than in *Ilf3*$^{+/+}$ mice under WIRS (Figures 3N and 3O; Tables S8A and S9A). This, along with the unique downregulation of *mt-Nd6* (Figure S4O), was validated by quantitative RT-PCR (Figures S4L–S4N). However, the mRNA expression response to WIRS in the *Ilf3*$^{\Delta PrLD/\Delta PrLD}$ mice was markedly altered with little correlation to that in the *Ilf3*$^{+/+}$ mice

Table 1. Comprehensive behavioral test battery of *Ilf3*$^{\Delta PrLD/\Delta PrLD}$ mice

Test	Age (w)	Phenotypes in *Ilf3*$^{\Delta PrLD/\Delta PrLD}$ mice	Figures
Body weight and body temperature	11-12	Decreased body weight, increased body temperature	4
Grip strength	11-12	N.S.	S5
Wire hang	11-12	N.S.	S5
Light/dark transition test	11-12	Hyperactivity, decreased anxiety-like behavior	4
Open field test	12	Hyperactivity, decreased anxiety-like behavior	4
Elevated plus maze	12	Hyperactivity	S6
Hot plate test	12	N.S.	S5
Social interaction test in a novel environment	12-13	Hyperactivity, decreased duration of contact	S7
Rotarod test	13	N.S.	S5
Three-chamber social approach test (100 lux)	15-16	Hyperactivity	S7
Acoustic startle response/prepulse inhibition test	16	Decreased startle	S6
Porsolt forced swim test	16	N.S.	S6
Barns maze test	22-30	Low task performance in trials after memory retention for a month	4 and S8
T-maze (spontaneous alternation)	30-31	High task performance	S8
Contextual and cued fear conditioning test	48-53	Deficits in fear conditioning memory	4 and S8
Three-chamber social approach test (5 lux)	65-66	Hyperactivity	S7
Social interaction test in a home cage	82-83	Hyperactivity	S7
Tail suspension	85	Depression-like behavior	S6

N.S.: no significant differences.

(Figure 3M; Table S6A). These results suggested that the deletion of NFAR2 PrLD altered the mRNA expression dependence on chronic stress in mouse AMY.

To survey the impact of WIRS and PrLD deletion on protein synthesis, we conducted ribosome profiling[46,47] from the same materials (Figure 3A). Essentially, we observed similar trends of alteration in translation (Figures 3P–3R; Table S5B) as found in mRNA (Figures 3J–3L; Table S5A): high similarities among WIRS, PrLD deletion, and the combinational effects. We also noticed that, as found in RNA-seq (Figure 3M; Table S6A), the response of the *Ilf3*$^{\Delta PrLD/\Delta PrLD}$ mice to WIRS was significantly altered from that of *Ilf3*$^{+/+}$ mice (Figure 3S; Table S6B). Interestingly, mRNA expression changes were not always reflected in the protein synthesis of the mRNAs (Figures 3F–3I and S4D–S4F; Tables S3A–S3D and S4A–S4C). Indeed, we noticed that a subset of WIRS-responsive mRNAs was translationally buffered in WIRS in both the genotypes (Figures S4G–S4I; Tables S7A–S7C). Nonetheless, *Mt* and *Hb* genes were actively translated upon mRNA accumulation by the combination of PrLD deletion and WIRS (Figures 3T, 3U, S4J, and S4K; Tables S8A–S8C and S9A–S9C), which was reflected in the GO enrichment analysis (Figure S4F; Table S4C). These results suggested that the NFAR2 PrLD deletion altered the translational responsiveness to chronic stress. Taken together, our data suggested that the loss of NFAR2 PrLD mimics stress-induced transcriptome and translatome alterations without WIRS and alters WIRS-responsive control of mRNA expression and translation in mouse AMY (Figure S4R).

Ilf3$^{\Delta PrLD/\Delta PrLD}$ mice show increased body temperature and activity, reduced anxiety-like behavior, and impaired conditioned fear memory

Next, we investigated the functional role of NFAR2 PrLD in mouse behavior using the comprehensive battery of behavioral tests[48,49] (Table 1). First, *Ilf3*$^{\Delta PrLD/\Delta PrLD}$ mice had comparable physical and sensory abilities (Figure S5), but they showed weight loss, increased body temperature, and increased activity compared with wild-type littermates (Figures 4A, 4B, 4D, 4H, S6A, S6C, S7D–S7F, S7J, S7K, S7O, S7P, S7T, S7U, and S7Y; Table 1). Second, the *Ilf3*$^{\Delta PrLD/\Delta PrLD}$ mice showed reduced anxiety-like behavior in the open field test (Figure 4F) and the light/dark transition test (Figures 4H–4K). Third, the *Ilf3*$^{\Delta PrLD/\Delta PrLD}$ mice and the wild-type controls showed similar performance in the T-maze and the Barnes maze (Figures 4L–4N, S8A, and S8D–S8F). However,

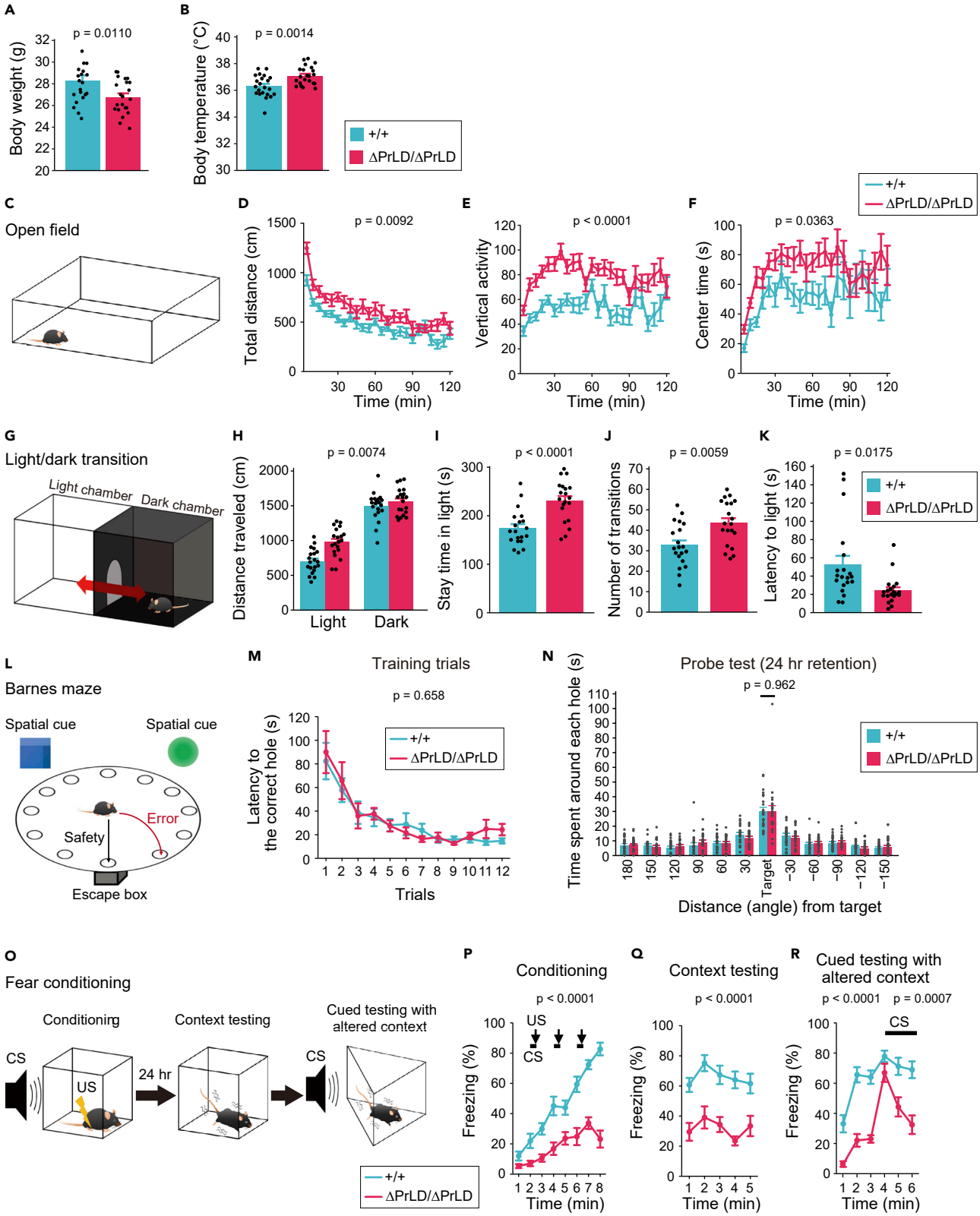
A
Body weight (g)
p = 0.0110
B
Body temperature (°C)
p = 0.0014
+/+
ΔPrLD/ΔPrLD
C
Open field
D
Total distance (cm)
p = 0.0092
Time (min)
E
Vertical activity
p < 0.0001
Time (min)
F
Center time (s)
p = 0.0363
Time (min)
G
Light/dark transition
Light chamber
Dark chamber
H
Distance traveled (cm)
p = 0.0074
Light
Dark
I
Stay time in light (s)
p < 0.0001
J
Number of transitions
p = 0.0059
K
Latency to light (s)
p = 0.0175
L
Barnes maze
Spatial cue
Spatial cue
Error
Safety
Escape box
M
Training trials
p = 0.658
Latency to the correct hole (s)
Trials
N
Probe test (24 hr retention)
p = 0.962
Time spent around each hole (s)
Target
Distance (angle) from target
O
Fear conditioning
Conditioning
Context testing
Cued testing with altered context
CS
US
24 hr
P
Conditioning
p < 0.0001
Freezing (%)
Time (min)
Q
Context testing
p < 0.0001
R
Cued testing with altered context
p < 0.0001
p = 0.0007

Figure 4. *Ilf3*$^{\Delta PrLD/\Delta PrLD}$ mice show increased body temperature and activity, reduced anxiety, and impaired conditioned fear memory

(A and B) Body weight (A) and temperature (B). n = 22.

(C–F) Open field test. Total distance traveled (D), vertical activity (E), and time spent in the center area of the field (F). n = 22.

(G–K) Light/dark transition test. Total distance traveled (H), time spent in the light chamber (I), number of transitions (J), and latency to first entry into the light chamber (K). n = 20.

(L–N) Barnes maze test. The latency to the correct hole in the training session (M) and the time spent around each hole in the probe trial conducted 24 h after the last training (N). n = 22.

(O–R) Fear conditioning test. CS, conditioned stimuli (white noise); US, unconditioned stimuli (foot shock). Freezing response was measured during conditioning (P), contextual test (Q), and cued test (R). Bars and arrows indicate the time when CS and US were presented, respectively. n = 22.

The data are presented as mean ± SEM. The p values in one-way ANOVA (A, B, H–K, and N) and the genotype effect in two-way repeated measures ANOVA (D–F, M, and P–R) are shown.

See also Table 1 and Figures S5–S8.

the *Ilf3*$^{\Delta PrLD/\Delta PrLD}$ mice showed attenuated fear responses in the contextual and cued fear conditioning test (Figures 4O–4R, S8G, and S8H). These changes in emotion- and fear-associated responses suggested that AMY-related neural networks and function were affected.[50,51]

To trace the neural activity in the fear conditioning test, mice were immunostained for c-Fos, a marker of neural activation, in the AMY, dHIP, and vHIP (Figure 5A). In *Ilf3*$^{+/+}$ mice, foot shock (FS) caused a mild increase in c-Fos-positive cells in the dHIP and a significant increase in the AMY and vHIP (Figures 5B–5J). Whereas *Ilf3*$^{\Delta PrLD/\Delta PrLD}$ mice had similar accumulations of c-Fos-positive cells in the AMY and dHIP (Figures 5B and 5D–5H), vHIP of the mice lost the response (Figures 5C, 5I, and 5J). Since the vHIP and AMY are structurally and functionally connected to encode emotion and fear,[52,53] the failure of the vHIP in *Ilf3*$^{\Delta PrLD/\Delta PrLD}$ mice to activate in response to FS may be associated with the alterations in the AMY and underlie the attenuated fear responses in those mice. In the context of neural connection, the delayed early development of axons in cultured neurons from the AMY of *Ilf3*$^{\Delta PrLD/\Delta PrLD}$ mice might be related to such defects in connectivity (Figure S9).

Prion-like domain of NFAR2 confers tolerance to chronic stress in forming conditioned fear memory

Next, to investigate the behavior outcome associated with WIRS, we applied the Morris water maze and passive avoidance tests to mice with WIRS (Figure 6A). The former test showed that PrLD deletion did not affect spatial learning and memory (Figures 6B and 6C), consistent with the Barnes maze test (Figures 4L–4N). In contrast, the passive avoidance test demonstrated that *Ilf3*$^{\Delta PrLD/\Delta PrLD}$ mice spent significantly longer time than *Ilf3*$^{+/+}$ mice in a dark chamber where the mice had received the FS (Figure 6D). This indicates that PrLD deletion affected conditioned fear memory, as was the case with the contextual and cued fear conditioning test (Figures 4O–4R). Notably, although the dark chamber avoidance behavior of *Ilf3*$^{+/+}$ mice was unaffected by WIRS, WIRS exacerbated the avoidance behavior of *Ilf3*$^{\Delta PrLD/\Delta PrLD}$ mice (Figures 6D and S11F). These results suggested that PrLD deletion had an impact on both conditioned fear memory and tolerance to WIRS in the formation of conditioned fear memory.

To more precisely identify the PrLD-specific role in conditioned fear memory and stress tolerance, we perturbed the overall expression levels of NFARs and NFAR2ΔPrLD in mice and investigated the behavioral changes. To this end, we generated *Ilf3*$^{+/-}$ and *Ilf3*$^{\Delta PrLD/-}$ mice using CRISPR/Cas9. The genome editing deleted 14 bp in exon 7, resulting in a frameshift mutation generating a downstream premature stop codon in exon 9 (Figures S10A–S10C). The mutated *Ilf3* allele (*Ilf3*$^{-}$) encoded amino acid residues 1-224, followed by mutated residues 225-263 (Figure S10C). Since Western blotting using a polyclonal antibody against the N terminus of ILF3 did not detect such low molecular weight proteins (Figure S10G), few proteins were translated and/or accumulated from the *Ilf3*$^{-}$ allele. As a result, the expression levels of NFARs were reduced by 30-50% in the brains of the *Ilf3*$^{+/-}$ and *Ilf3*$^{\Delta PrLD/-}$ mice compared with the *Ilf3*$^{+/+}$ and *Ilf3*$^{\Delta PrLD/\Delta PrLD}$ mice, respectively (Figures S10H–S10J).

In the Morris water maze, the *Ilf3*$^{\Delta PrLD/-}$ mice required longer escape latency than *Ilf3*$^{+/+}$ mice, but the latency decreased with increasing trials, and the performance of the mice in probe tests was equivalent to *Ilf3*$^{+/+}$ mice (Figures 6E and 6F). These results showed that neither loss of PrLD nor decreased expression of NFAR2ΔPrLD had a significant effect on spatial learning and memory. In contrast, in the passive avoidance test, the *Ilf3*$^{\Delta PrLD/-}$ mice entered the dark chamber as early as 5 min after FS (Figure 6G). This inability to fully learn the context made it impossible to evaluate the WIRS-caused exacerbations as observed in the

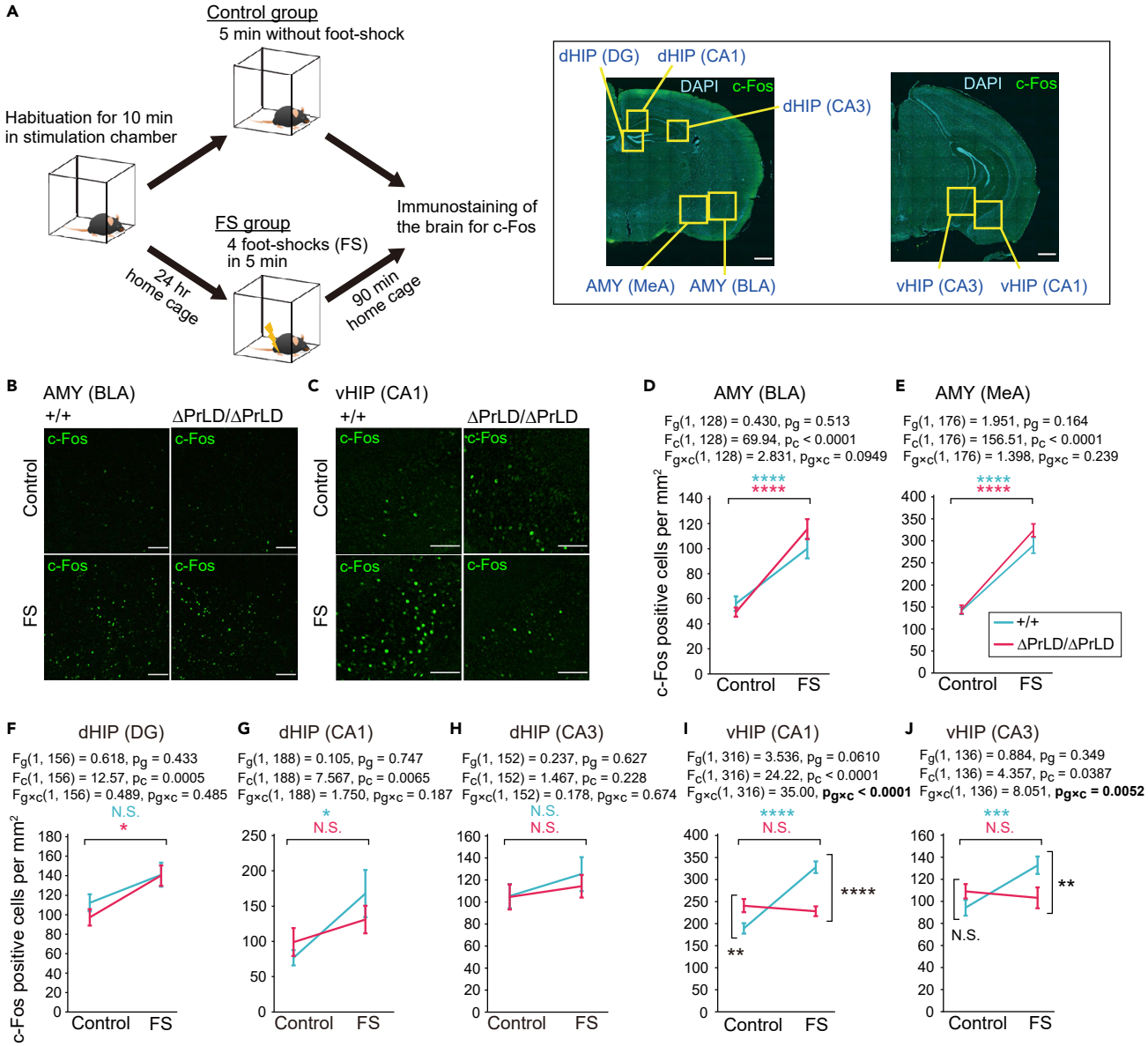

Figure 5. Fear-induced upregulation of c-Fos in the vHIP is lost in *Ilf3*$^{\Delta PrLD/\Delta PrLD}$ mice

(A) Schematic of immunostaining for c-Fos after foot shock (FS). The right panels are brain slices double-stained with DAPI and c-Fos, showing the brain regions. MeA, medial amygdala; BLA, basolateral amygdala. Scale bars, 1 mm.

(B and C) c-Fos in the AMY (B) and vHIP (C) of *Ilf3*$^{+/+}$ and *Ilf3*$^{\Delta PrLD/\Delta PrLD}$ mice with and without FS. Scale bars, 100 μm.

(D–J) Quantification of c-Fos positive cells. The data are presented as mean ± SEM. n = 33 (D), 45 (E), 40 (F), 48 (G), 39 (H), 80 (I), and 35 (J) pictures from four mice in each group. The data were analyzed using two-way ANOVA. The F-values and p values for the main effect of genotypes (F_g and p_g, respectively), stimuli (with or without FS) (F_c and p_c, respectively), and interaction between genotypes and stimuli ($F_{g\times c}$ and $p_{g\times c}$, respectively) are shown. In D-H, ****p < 0.0001, *p < 0.05 in Tukey-Kramer test after the two-way ANOVA. In I and J, ****p < 0.0001, ***p < 0.001, **p < 0.01 in simple effect analysis after significant interaction in the two-way ANOVA. N.S., no significant difference (p ≥ 0.05).

See also Figure S9.

Ilf3$^{\Delta PrLD/\Delta PrLD}$ mice (Figure 6D). This NFAR2ΔPrLD-dose dependence of conditioned fear memory formation suggested that the loss of conditioned fear memory is caused not specifically by the deletion of the PrLD.

Also, the reduced expression of both NFAR1 and NFAR2 in the *Ilf3*$^{+/-}$ mice did not significantly affect spatial learning and memory in the Morris water maze (Figures 6H and 6I). In contrast, these mice had impaired memory in the passive avoidance test (Figure 6J). This indicated that the loss of conditioned fear memory

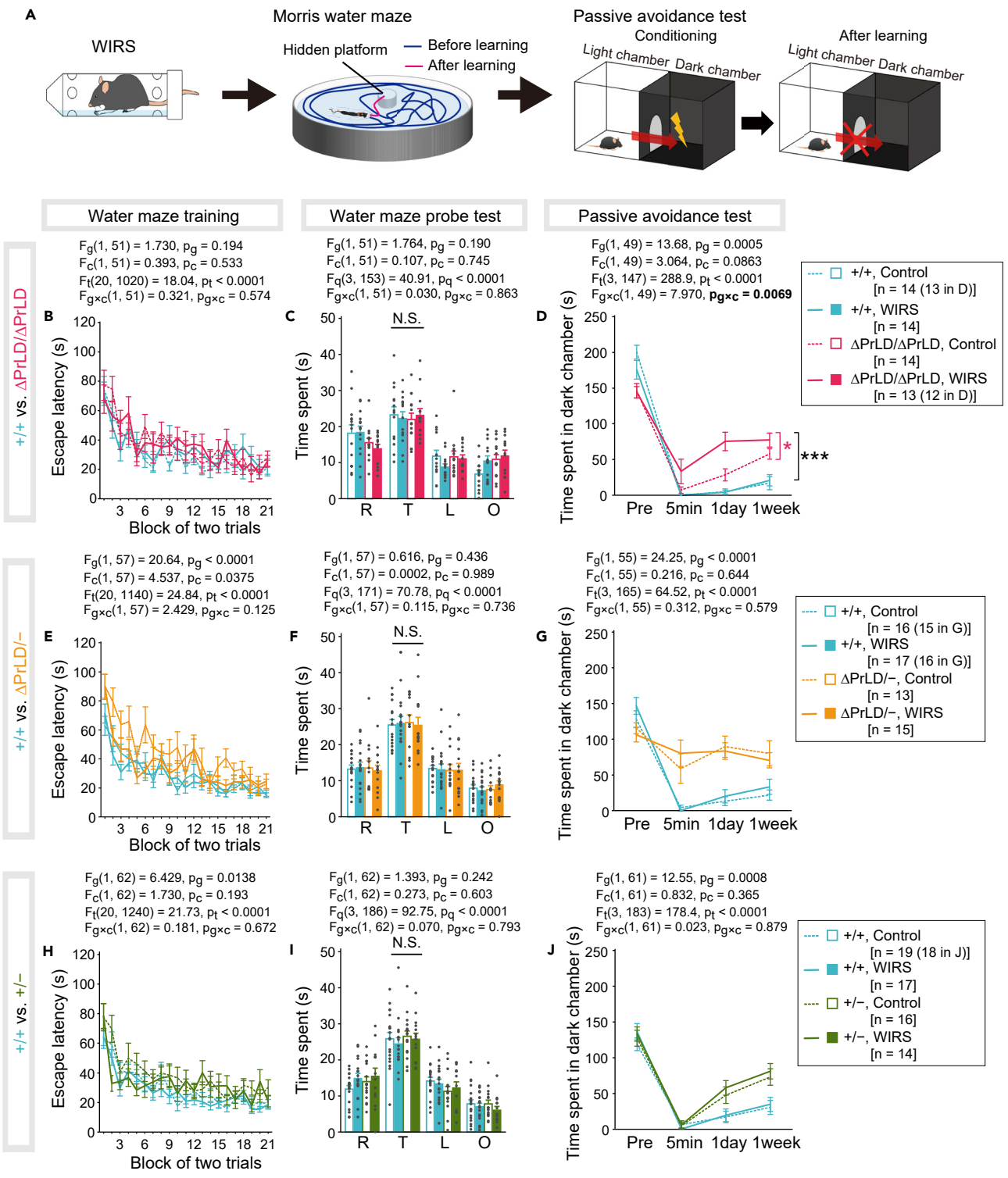

Figure 6. *Ilf3*$^{\Delta PrLD/\Delta PrLD}$ mice are highly sensitive to WIRS in conditioned fear memory formation

(A) Mice were exposed to WIRS and subsequently underwent the Morris water maze and fear conditioning (passive avoidance) tests.

(B and C) Results for *Ilf3*$^{+/+}$ and *Ilf3*$^{\Delta PrLD/\Delta PrLD}$ mice in the Morris water maze. Escape latency to the platform in the training session (B) and time spent in each quadrant in the probe test conducted one day after the last training (C). R, right; T, target; L, left; O, opposite quadrants.

(D) Results for *Ilf3*$^{+/+}$ and *Ilf3*$^{\Delta PrLD/\Delta PrLD}$ mice in the passive avoidance test. Time spent in the dark chamber before FS (Pre) and 5 min, 1 day, and 1 week after the conditioning.

Figure 6. *Continued*
(E–G) Results for *Ilf3*$^{+/+}$ and *Ilf3*$^{\Delta PrLD/-}$ mice.
(H–J) Results for *Ilf3*$^{+/+}$ and *Ilf3*$^{+/-}$ mice.
The data were analyzed using three-way repeated measures ANOVA. The F-values and p values for the main effects of genotype (F_g and p_g, respectively), condition (with or without WIRS) (F_c and p_c, respectively), trial (F_t and p_t, respectively), and quadrant (F_q and p_q, respectively), and the interaction effect between genotype and condition ($F_{g\times c}$ and $p_{g\times c}$, respectively) are indicated. N.S., no significant difference. In D, ***$p < 0.001$, *$p < 0.05$ in simple effect analysis after significant interaction in the three-way repeated measures ANOVA.
See also Figures S10 and S11.

is caused also by the reduction in the amount of NFARs. However, conditioned fear memory in the *Ilf3*$^{+/-}$ mice showed no sensitivity to WIRS (Figures 6J and S11L), which was in contrast to the results in *Ilf3*$^{\Delta PrLD/\Delta PrLD}$ mice, whose conditioned fear memory was exacerbated by WIRS (Figures 6D and S11F). In summary, comparisons of the *Ilf3* mutants and wild-type mice suggested that both NFAR1 and NFAR2 are involved in fear-conditioned memory formation regardless of the PrLD, whereas the presence of the PrLD in NFAR2 is required specifically for tolerance of mice to chronic stress in the formation of conditioned fear memory.

DISCUSSION

Our study demonstrated that PrLD deletion in NFAR2 reduced the tolerance of mice to WIRS in the formation of fear-associated memories. This behavioral outcome was associated with molecular phenotypes in the AMY; the reduction in the WIRS-sensitive nuclear retention of NFARs and the alteration in WIRS-induced gene expression changes. Remarkably, the transcriptional and translational profiles induced by WIRS differed between *Ilf3*$^{+/+}$ and *Ilf3*$^{\Delta PrLD/\Delta PrLD}$ mice. Given these results, we hypothesize that the insertion of the PrLD into NFAR2 confers molecular interactions for nuclear retention which may impact WIRS-responsive spatiotemporal regulation of mRNA expression and translation by NFARs. These controls by the PrLD may increase the tolerance of AMY and its associated nervous system to WIRS and, as a result, the tolerance of mice to WIRS in conditioned fear memory formation.

This study showed that PrLD of NFAR2 is required for nuclear retention, rather than condensate formation. Although PrLD has been recognized as aggregation-prone, a recent study challenges this stereotype: the PrLD of TDP-43 is required to prevent, rather than promote, the formation of speckle-like structures in the nucleus.[54] Since comprehensive identification of PrLD-containing proteins showed their association with nucleoplasmic localization,[55] retention in the nucleoplasm, rather than the formation of condensates, may be a common feature of PrLDs in these proteins.

The reduced nuclear retention of NFARs by PrLD deletion may resemble stress conditions because the export of NFARs from the nucleus to the cytoplasm is facilitated by cellular stress.[22,32] In addition, the correlation between the PrLD deletion-caused gene expression changes and the WIRS-induced gene expression changes suggests that the PrLD-deficient mice are in a stress-like state even without WIRS. This notion may be supported by the results showing that *Ilf3*$^{\Delta PrLD/\Delta PrLD}$ mice exhibited elevated body temperature and hyperactivity, similar to those caused by chronic stress.[56,57] This stress-reminiscent state of PrLD-deficient mice and the misregulation of WIRS-induced gene expression could affect the response to WIRS and stress tolerance. In relation to this model, translation of mRNAs included in the GO terms of "Oxidative phosphorylation" and "Cellular oxidant detoxification" was increased in the AMY of *Ilf3*$^{\Delta PrLD/\Delta PrLD}$ mice under WIRS, suggesting that those processes were compromised.

Both *Ilf3*$^{\Delta PrLD/\Delta PrLD}$ and *Ilf3*$^{+/-}$ mice reduced conditioned fear memory compared with *Ilf3*$^{+/+}$ mice in the absence of WIRS, suggesting that NFARs are involved in fear memory formation in a PrLD-nonspecific manner. However, exacerbation of conditioned fear memory under WIRS occurred only in *Ilf3*$^{\Delta PrLD/\Delta PrLD}$ mice, but not in *Ilf3*$^{+/-}$ mice, suggesting that PrLD conferred stress tolerance on fear memories. At the cellular level, the effects of PrLD deletion on FS-induced neural activity and WIRS sensitivity were evident in different brain regions, vHIP and AMY, respectively (Figures 2 and 5). These raise the following models: 1) FS-induced neural activity in vHIP may be NFARs-mediated in a PrLD-nonspecific manner and may be NFARs dose-dependent, contributing to fear memory formation, and 2) Chronic stress sensitivity in the AMY is specifically dependent on the PrLD, which regulates the chronic stress tolerance of fear memory. Considering that vHIP and AMY are structurally and functionally connected to regulate fear-associated memory, it is possible that AMY's stress sensitivity might influence neural circuits including vHIP that control fear memory formation. Nevertheless, RNA-seq in the AMY identified WIRS-induced expression changes not only in stress-related genes, but also in genes related to fear-conditioned memory, such as

Lsamp and *Bptf* (a.k.a. fetal Alzheimer antigen) (Tables S1A, S1C, and S1D).[58,59] This suggests that the role of the AMY may be more complex than simply modulating stress sensitivity. At the cellular level, Lsamp is involved in axon outgrowth and targeting,[60] which was coincident with the result that cultured neurons from *Ilf3*$^{\Delta PrLD/\Delta PrLD}$ AMY showed delayed development of axons. Alternative models may therefore include a more direct role for NFAR2 PrLD in the AMY in conditioned fear memory formation, where the loss of the PrLD could impair the output of neural activity from AMY to vHIP, which may be exacerbated by WIRS.

It is noteworthy that *Ilf3*$^{\Delta PrLD/\Delta PrLD}$ and *Ilf3*$^{+/-}$ mice showed memory impairment in fear conditioning, but not in spatial tasks. Although the reason for this difference was unknown, similar behavioral phenotypes have been reported for RNA granule-associated proteins such as FXR2 and Ataxin-2.[61,62] Fear conditioning depends on the AMY and vHIP, whereas spatial memory depends on the dHIP. The AMY and vHIP may be more sensitive than the dHIP to changes in gene expression caused by the misregulation of these RNA-binding proteins and thus leads to behavioral abnormality in fear. Alternatively, fear conditioning can be more stressful to mice than spatial tasks, requiring stress-responsive regulation of gene expression by these RNA-binding proteins. PrLD of NFAR2 may act as an adaptive switch that enables normal AMY-related behaviors even in stressful environments. This role is reminiscent of those of yeast and plant PrLDs in responding to fluctuating environments.[13–15] Therefore, it is an interesting question of whether other PrLDs in various proteins also contribute to adaptation to the environment.

Like NFARs, alternative splicing of PrLDs occurs in many proteins such as TDP-43 and hnRNP A1.[63,64] These splicing isoforms differ in the ability to form pathogenic aggregates,[63,64] supporting the idea that the insertion (and deletion) of PrLDs is the basis for the diversification of protein functions. There may be some trade-offs between the physiological advantages and pathological disadvantages. Here, in the case of NFAR2, we have shown the physiological relevance of the PrLD: the NFRA2 PrLD regulates chronic stress-induced gene expression changes and is required for tolerance of conditioned fear memory to chronic stress. However, it is still unclear whether PrLD-deficient NFAR1 also needs to be synthesized. Solving these questions about PrLD-containing proteins will lead to a better understanding of the advantages and disadvantages of the presence of PrLDs and their trade-offs.

Limitations of the study

First, we were unable to detect the subcellular localization of NFAR1 and NFAR2 individually. In addition, we could not distinguish between NFAR1 and NFAR2ΔPrLD in *Ilf3*$^{\Delta PrLD/\Delta PrLD}$ mice. These were due to the use of the anti-ILF3 antibody that detects both NFAR1 and NFAR2, as specific antibodies against each of them do not currently exist. One solution is to generate antibodies specific for the C-terminal 15 amino acids of NFAR1 and against PrLD of NFAR2. This enables to analyze the differences in the intracellular behavior of NFAR1 and NFAR2 under WIRS between *Ilf3*$^{+/+}$ and *Ilf3*$^{\Delta PrLD/\Delta PrLD}$ mice, allowing us to better understand their functional differences in the presence or absence of PrLD.

Second, we used conventional mutant mice, which limited the analysis of brain region-specific effects of NFAR2 PrLD deletion and NFAR2 deficiency. Future generation and analysis of conditional mutant mice, in which deletions of PrLD and NFAR2 occur at favorable times in targeted cell types, will reveal specific roles for NFAR2 PrLD that may differ in different brain regions such as AMY and vHIP.

STAR★METHODS

Detailed methods are provided in the online version of this paper and include the following:

- KEY RESOURCES TABLE
- RESOURCE AVAILABILITY
  - Lead contact
  - Material availability
  - Data and code availability
- EXPERIMENTAL MODEL AND SUBJECT DETAILS
  - Mice
- METHOD DETAILS
  - Phylogenetic analysis of DZF-containing proteins
  - IDR and PrLD predictions
  - Generation of ILF3 PrLD-deficient mice

SUPPLEMENTAL INFORMATION

Supplemental information can be found online at https://doi.org/10.1016/j.isci.2023.106229.

ACKNOWLEDGMENTS

We thank C. Matsuda for technical assistance; S. Ohsawa for the generation of the ILF3 deficient mice; Dr. H. Koyama for advice on image analysis; Model Organisms, Trans-Omics, and Optics and Imaging Facilities in the Trans-scale Biology Center of the National Institute for Basic Biology for technical supports. This work was supported by a Life Science Research grant from RIKAKEN HOLDINGS CO., LTD. and the Sasakawa Scientific Research Grant from The Japan Science Society (2020-4061) to A.Y.; Grant-in-Aid for Early-Career Scientists (JP21K15023) from the Japan Society for the Promotion of Science (JSPS), Grant-in-Aid for Transformative Research Areas [A] (JP21H05734) from the Ministry of Education, Culture, Sports, Science and Technology (MEXT), and Special Postdoctoral Researchers and Incentive Research Projects from RIKEN to Y.S.; Grant-in-Aid for Scientific Research (JP19H02959) from the JSPS, Grant-in-Aid for Transformative Research Areas [B] (JP20H05784) from the MEXT, AMED-CREST (JP21gm1410003) from the Japan Agency for Medical Research and Development (AMED), and "Biology of Intracellular Environments" and "Integrated life science research to challenge super aging society" from RIKEN to S.I; Grant-in-Aid for Scientific Research (19H03161, 22H02552 and 16H06276 (AdAMS)) from the JSPS and the Bioscience Research Grant from the Takeda Science Foundation to N.S.

AUTHOR CONTRIBUTIONS

A.Y. designed the research, performed experiments, analyzed the data, and wrote the article. Y.S. and S.I. provided guidance and support in RNA-seq and ribosome profiling and edited the article. M.M. supported RNA-seq and ribosome profiling and generated ILF3 PrLD-deficient mice. S. N. generated ILF3 PrLD-deficient mice and contributed to the writing. K.F., Y.K., M.A., E.S., and K.T. performed the behavioral test battery. N.S. conceived and supervised the research and wrote the article.

DECLARATION OF INTERESTS

The authors declare no competing interests.

INCLUSION AND DIVERSITY

We support inclusive, diverse, and equitable conduct of research.

Received: October 6, 2022
Revised: January 11, 2023
Accepted: February 14, 2023
Published: February 19, 2023

REFERENCES

1. Haynes, C., Oldfield, C.J., Ji, F., Klitgord, N., Cusick, M.E., Radivojac, P., Uversky, V.N., Vidal, M., and Iakoucheva, L.M. (2006). Intrinsic disorder is a common feature of hub proteins from four eukaryotic interactomes. PLoS Comput. Biol. *2*, e100. https://doi.org/10.1371/journal.pcbi.0020100.

2. Shimizu, K., and Toh, H. (2009). Interaction between intrinsically disordered proteins frequently occurs in a human protein-protein interaction network. J. Mol. Biol. *392*, 1253–1265. https://doi.org/10.1016/j.jmb.2009.07.088.

3. Uversky, V.N. (2017). Intrinsically disordered proteins in overcrowded milieu: membrane-less organelles, phase separation, and intrinsic disorder. Curr. Opin. Struct. Biol. *44*, 18–30. https://doi.org/10.1016/j.sbi.2016.10.015.

4. Gomes, E., and Shorter, J. (2019). The molecular language of membraneless organelles. J. Biol. Chem. *294*, 7115–7127. https://doi.org/10.1074/jbc.TM118.001192.

5. Boeynaems, S., Alberti, S., Fawzi, N.L., Mittag, T., Polymenidou, M., Rousseau, F., Schymkowitz, J., Shorter, J., Wolozin, B., Van Den Bosch, L., et al. (2018). Protein phase separation: a new phase in cell biology. Trends Cell Biol. *28*, 420–435. https://doi.org/10.1016/j.tcb.2018.02.004.

6. Woodruff, J.B., Hyman, A.A., and Boke, E. (2018). Organization and function of non-dynamic biomolecular condensates. Trends Biochem. Sci. *43*, 81–94. https://doi.org/10.1016/j.tibs.2017.11.005.

7. Kato, M., Han, T.W., Xie, S., Shi, K., Du, X., Wu, L.C., Mirzaei, H., Goldsmith, E.J., Longgood, J., Pei, J., et al. (2012). Cell-free formation of RNA granules: low complexity sequence domains form dynamic fibers within hydrogels. Cell *149*, 753–767. https://doi.org/10.1016/j.cell.2012.04.017.

8. Ling, S.C., Polymenidou, M., and Cleveland, D.W. (2013). Converging mechanisms in ALS and FTD: disrupted RNA and protein homeostasis. Neuron *79*, 416–438. https://doi.org/10.1016/j.neuron.2013.07.033.

9. Portz, B., Lee, B.L., and Shorter, J. (2021). FUS and TDP-43 phases in health and disease. Trends Biochem. Sci. *46*, 550–563. https://doi.org/10.1016/j.tibs.2020.12.005.

10. Wang, J., Choi, J.M., Holehouse, A.S., Lee, H.O., Zhang, X., Jahnel, M., Maharana, S., Lemaitre, R., Pozniakovsky, A., Drechsel, D., et al. (2018). A molecular grammar governing the driving forces for phase separation of prion-like RNA binding proteins. Cell *174*, 688–699.e16. https://doi.org/10.1016/j.cell.2018.06.006.

11. Franzmann, T.M., and Alberti, S. (2019). Prion-like low-complexity sequences: key regulators of protein solubility and phase behavior. J. Biol. Chem. *294*, 7128–7136. https://doi.org/10.1074/jbc.TM118.001190.

12. Maharana, S., Wang, J., Papadopoulos, D.K., Richter, D., Pozniakovsky, A., Poser, I., Bickle, M., Rizk, S., Guillén-Boixet, J., Franzmann, T.M., et al. (2018). RNA buffers the phase separation behavior of prion-like RNA binding proteins. Science *360*, 918–921. https://doi.org/10.1126/science.aar7366.

13. Halfmann, R., Jarosz, D.F., Jones, S.K., Chang, A., Lancaster, A.K., and Lindquist, S. (2012). Prions are a common mechanism for phenotypic inheritance in wild yeasts. Nature *482*, 363–368. https://doi.org/10.1038/nature10875.

14. Jung, J.H., Barbosa, A.D., Hutin, S., Kumita, J.R., Gao, M., Derwort, D., Silva, C.S., Lai, X., Pierre, E., Geng, F., et al. (2020). A prion-like domain in ELF3 functions as a thermosensor in Arabidopsis. Nature *585*, 256–260. https://doi.org/10.1038/s41586-020-2644-7.

15. Dorone, Y., Boeynaems, S., Flores, E., Jin, B., Hateley, S., Bossi, F., Lazarus, E., Pennington, J.G., Michiels, E., De Decker, M., et al. (2021). A prion-like protein regulator of seed germination undergoes hydration-dependent phase separation. Cell *184*, 4284–4298.e27. https://doi.org/10.1016/j.cell.2021.06.009.

16. Xue, B., Dunker, A.K., and Uversky, V.N. (2012). Orderly order in protein intrinsic disorder distribution: disorder in 3500 proteomes from viruses and the three domains of life. J. Biomol. Struct. Dyn. *30*, 137–149. https://doi.org/10.1080/07391102.2012.675145.

17. Niklas, K.J., Dunker, A.K., and Yruela, I. (2018). The evolutionary origins of cell type diversification and the role of intrinsically disordered proteins. J. Exp. Bot. *69*, 1437–1446. https://doi.org/10.1093/jxb/erx493.

18. Romero, P.R., Zaidi, S., Fang, Y.Y., Uversky, V.N., Radivojac, P., Oldfield, C.J., Cortese, M.S., Sickmeier, M., LeGall, T., Obradovic, Z., and Dunker, A.K. (2006). Alternative splicing in concert with protein intrinsic disorder enables increased functional diversity in multicellular organisms. Proc. Natl. Acad. Sci. USA *103*, 8390–8395. https://doi.org/10.1073/pnas.0507916103.

19. Dunker, A.K., Oldfield, C.J., Meng, J., Romero, P., Yang, J.Y., Chen, J.W., Vacic, V., Obradovic, Z., and Uversky, V.N. (2008). The unfoldomics decade: an update on intrinsically disordered proteins. BMC Genom. *9* (*Suppl 2*), S1. https://doi.org/10.1186/1471-2164-9-S2-S1.

20. Niklas, K.J., Bondos, S.E., Dunker, A.K., and Newman, S.A. (2015). Rethinking gene regulatory networks in light of alternative splicing, intrinsically disordered protein domains, and post-translational modifications. Front. Cell Dev. Biol. *3*, 8. https://doi.org/10.3389/fcell.2015.00008.

21. Babu, M.M. (2016). The contribution of intrinsically disordered regions to protein function, cellular complexity, and human disease. Biochem. Soc. Trans. *44*, 1185–1200. https://doi.org/10.1042/BST20160172.

22. Harashima, A., Guettouche, T., and Barber, G.N. (2010). Phosphorylation of the NFAR proteins by the dsRNA-dependent protein kinase PKR constitutes a novel mechanism of translational regulation and cellular defense. Genes Dev. *24*, 2640–2653. https://doi.org/10.1101/gad.1965010.

23. Duchange, N., Pidoux, J., Camus, E., and Sauvaget, D. (2000). Alternative splicing in the human interleukin enhancer binding factor 3 (ILF3) gene. Gene *261*, 345–353. https://doi.org/10.1016/s0378-1119(00)00495-9.

24. Batlle, C., de Groot, N.S., Iglesias, V., Navarro, S., and Ventura, S. (2017). Characterization of soft amyloid cores in human prion-like proteins. Sci. Rep. *7*, 12134. https://doi.org/10.1038/s41598-017-09714-z.

25. Castella, S., Bernard, R., Corno, M., Fradin, A., and Larcher, J.C. (2015). Ilf3 and NF90 functions in RNA biology. Wiley Interdiscip. Rev. RNA *6*, 243–256. https://doi.org/10.1002/wrna.1270.

26. Parrott, A.M., Walsh, M.R., Reichman, T.W., and Mathews, M.B. (2005). RNA binding and

phosphorylation determine the intracellular distribution of nuclear factors 90 and 110. J. Mol. Biol. *348*, 281–293. https://doi.org/10.1016/j.jmb.2005.02.047.

27. Pfeifer, I., Elsby, R., Fernandez, M., Faria, P.A., Nussenzveig, D.R., Lossos, I.S., Fontoura, B.M.A., Martin, W.D., and Barber, G.N. (2008). NFAR-1 and -2 modulate translation and are required for efficient host defense. Proc. Natl. Acad. Sci. USA *105*, 4173–4178. https://doi.org/10.1073/pnas.0711222105.

28. Kuwano, Y., Kim, H.H., Abdelmohsen, K., Pullmann, R., Jr., Martindale, J.L., Yang, X., and Gorospe, M. (2008). MKP-1 mRNA stabilization and translational control by RNA-binding proteins HuR and NF90. Mol. Cell Biol. *28*, 4562–4575. https://doi.org/10.1128/MCB.00165-08.

29. Agca, C., Boldt, K., Gubler, A., Meneau, I., Corpet, A., Samardzija, M., Stucki, M., Ueffing, M., and Grimm, C. (2015). Expression of leukemia inhibitory factor in Müller glia cells is regulated by a redox-dependent mRNA stability mechanism. BMC Biol. *13*, 30. https://doi.org/10.1186/s12915-015-0137-1.

30. Viranaicken, W., Gasmi, L., Chaumet, A., Durieux, C., Georget, V., Denoulet, P., and Larcher, J.C. (2011). L-Ilf3 and L-NF90 traffic to the nucleolus granular component: alternatively-spliced exon 3 encodes a nucleolar localization motif. PLoS One *6*, e22296. https://doi.org/10.1371/journal.pone.0022296.

31. Reichman, T.W., Parrott, A.M., Fierro-Monti, I., Caron, D.J., Kao, P.N., Lee, C.G., Li, H., and Mathews, M.B. (2003). Selective regulation of gene expression by nuclear factor 110, a member of the NF90 family of double-stranded RNA-binding proteins. J. Mol. Biol. *332*, 85–98. https://doi.org/10.1016/s0022-2836(03)00885-4.

32. Shiina, N., and Nakayama, K. (2014). RNA granule assembly and disassembly modulated by nuclear factor associated with double-stranded RNA 2 and nuclear factor 45. J. Biol. Chem. *289*, 21163–21180. https://doi.org/10.1074/jbc.M114.556365.

33. Zafir, A., and Banu, N. (2009). Modulation of in vivo oxidative status by exogenous corticosterone and restraint stress in rats. Stress *12*, 167–177. https://doi.org/10.1080/10253890802234168.

34. Schiavone, S., Jaquet, V., Trabace, L., and Krause, K.H. (2013). Severe life stress and oxidative stress in the brain: from animal models to human pathology. Antioxid. Redox Signaling *18*, 1475–1490. https://doi.org/10.1089/ars.2012.4720.

35. Pires-daSilva, A., Nayernia, K., Engel, W., Torres, M., Stoykova, A., Chowdhury, K., and Gruss, P. (2001). Mice deficient for spermatid perinuclear RNA-binding protein show neurologic, spermatogenic, and sperm morphological abnormalities. Dev. Biol. *233*, 319–328. https://doi.org/10.1006/dbio.2001.0169.

36. Lykke-Andersen, S., and Jensen, T.H. (2015). Nonsense-mediated mRNA decay: an intricate machinery that shapes transcriptomes. Nat. Rev. Mol. Cell Biol. *16*, 665–677. https://doi.org/10.1038/nrm4063.

37. Shi, L., Zhao, G., Qiu, D., Godfrey, W.R., Vogel, H., Rando, T.A., Hu, H., and Kao, P.N. (2005). NF90 regulates cell cycle exit and terminal myogenic differentiation by direct binding to the 3′-untranslated region of MyoD and p21WAF1/CIP1 mRNAs. J. Biol. Chem. *280*, 18981–18989. https://doi.org/10.1074/jbc.M411034200.

38. Jia, R., Ajiro, M., Yu, L., McCoy, P., Jr., and Zheng, Z.M. (2019). Oncogenic splicing factor SRSF3 regulates ILF3 alternative splicing to promote cancer cell proliferation and transformation. RNA *25*, 630–644. https://doi.org/10.1261/rna.068619.118.

39. Lee, Y.B., Scotter, E.L., Lee, D.Y., Troakes, C., Mitchell, J., Rogelj, B., Gallo, J.M., and Shaw, C.E. (2021). Cytoplasmic TDP-43 is involved in cell fate during stress recovery. Hum. Mol. Genet. *31*, 166–175. https://doi.org/10.1093/hmg/ddab227.

40. Allemand, E., Guil, S., Myers, M., Moscat, J., Cáceres, J.F., and Krainer, A.R. (2005). Regulation of heterogenous nuclear ribonucleoprotein A1 transport by phosphorylation in cells stressed by osmotic shock. Proc. Natl. Acad. Sci. USA *102*, 3605–3610. https://doi.org/10.1073/pnas.0409889102.

41. Yang, H., Xia, L., Chen, J., Zhang, S., Martin, V., Li, Q., Lin, S., Chen, J., Calmette, J., Lu, M., et al. (2019). Stress-glucocorticoid-TSC22D3 axis compromises therapy-induced antitumor immunity. Nat. Med. *25*, 1428–1441. https://doi.org/10.1038/s41591-019-0566-4.

42. Miyata, S., Koyama, Y., Takemoto, K., Yoshikawa, K., Ishikawa, T., Taniguchi, M., Inoue, K., Aoki, M., Hori, O., Katayama, T., and Tohyama, M. (2011). Plasma corticosterone activates SGK1 and induces morphological changes in oligodendrocytes in corpus callosum. PLoS One *6*, e19859. https://doi.org/10.1371/journal.pone.0019859.

43. Weger, M., Alpern, D., Cherix, A., Ghosal, S., Grosse, J., Russeil, J., Gruetter, R., de Kloet, E.R., Deplancke, B., and Sandi, C. (2020). Mitochondrial gene signature in the prefrontal cortex for differential susceptibility to chronic stress. Sci. Rep. *10*, 1018308. https://doi.org/10.1038/s41598-020-75326-9.

44. Schelshorn, D.W., Schneider, A., Kuschinsky, W., Weber, D., Krüger, C., Dittgen, T., Bürgers, H.F., Sabouri, F., Gassler, N., Bach, A., and Maurer, M.H. (2009). Expression of hemoglobin in rodent neurons. J. Cereb. Blood Flow Metab. *29*, 585–595. https://doi.org/10.1038/jcbfm.2008.152.

45. Stankiewicz, A.M., Goscik, J., Swiergiel, A.H., Majewska, A., Wieczorek, M., Juszczak, G.R., and Lisowski, P. (2014). Social stress increases expression of hemoglobin genes in mouse prefrontal cortex. BMC Neurosci. *15*, 130. https://doi.org/10.1186/s12868-014-0130-6.

46. Mito, M., Mishima, Y., and Iwasaki, S. (2020). Protocol for disome profiling to survey ribosome collision in humans and zebrafish. STAR Protoc. *1*, 100168. https://doi.org/10.1016/j.xpro.2020.100168.

47. Nakazawa, K., Shichino, Y., Iwasaki, S., and Shiina, N. (2020). Implications of RNG140 (caprin2)-mediated translational regulation in eye lens differentiation. J. Biol. Chem. *295*, 15029–15044. https://doi.org/10.1074/jbc.RA120.012715.

48. Takao, K., Tanda, K., Nakamura, K., Kasahara, J., Nakao, K., Katsuki, M., Nakanishi, K., Yamasaki, N., Toyama, K., Adachi, M., et al. (2010). Comprehensive behavioral analysis of calcium/calmodulin-dependent protein kinase IV knockout mice. PLoS One *5*, e9460. https://doi.org/10.1371/journal.pone.0009460.

49. Ohashi, R., Takao, K., Miyakawa, T., and Shiina, N. (2016). Comprehensive behavioral analysis of RNG105 (Caprin1) heterozygous mice: reduced social interaction and attenuated response to novelty. Sci. Rep. *6*, 20775. https://doi.org/10.1038/srep20775.

50. Phelps, E.A., and LeDoux, J.E. (2005). Contributions of the amygdala to emotion processing: from animal models to human behavior. Neuron *48*, 175–187. https://doi.org/10.1016/j.neuron.2005.09.025.

51. Babaev, O., Piletti Chatain, C., and Krueger-Burg, D. (2018). Inhibition in the amygdala anxiety circuitry. Exp. Mol. Med. *50*, 1–16. https://doi.org/10.1038/s12276-018-0063-8.

52. Fanselow, M.S., and Dong, H.W. (2010). Are the dorsal and ventral hippocampus functionally distinct structures? Neuron *65*, 7–19. https://doi.org/10.1016/j.neuron.2009.11.031.

53. Kim, W.B., and Cho, J.H. (2020). Encoding of contextual fear memory in hippocampal-amygdala circuit. Nat. Commun. *11*, 1382. https://doi.org/10.1038/s41467-020-15121-2.

54. Wang, I.F., Reddy, N.M., and Shen, C.K.J. (2002). Higher order arrangement of the eukaryotic nuclear bodies. Proc. Natl. Acad. Sci. USA *99*, 13583–13588. https://doi.org/10.1073/pnas.212483099.

55. March, Z.M., King, O.D., and Shorter, J. (2016). Prion-like domains as epigenetic regulators, scaffolds for subcellular organization, and drivers of neurodegenerative disease. Brain Res. *1647*, 9–18. https://doi.org/10.1016/j.brainres.2016.02.037.

56. Oka, T. (2015). Psychogenic fever: how psychological stress affects body temperature in the clinical population. Temperature (Austin) *2*, 368–378. https://doi.org/10.1080/23328940.2015.1056907.

57. Pardon, M.C., Kendall, D.A., Pérez-Diaz, F., Duxon, M.S., and Marsden, C.A. (2004). Repeated sensory contact with aggressive mice rapidly leads to an anticipatory increase in core body temperature and physical activity that precedes the onset of aversive responding. Eur. J. Neurosci. *20*, 1033–1050. https://doi.org/10.1111/j.1460-9568.2004.03549.x.

58. Lamprecht, R., Dracheva, S., Assoun, S., and LeDoux, J.E. (2009). Fear conditioning induces distinct patterns of gene expression in lateral amygdala. Gene Brain Behav. *8*, 735–743. https://doi.org/10.1111/j.1601-183X.2009.00515.x.

59. Innos, J., Philips, M.A., Raud, S., Lilleväli, K., Kõks, S., and Vasar, E. (2012). Deletion of the Lsamp gene lowers sensitivity to stressful environmental manipulations in mice. Behav. Brain Res. *228*, 74–81. https://doi.org/10.1016/j.bbr.2011.11.033.

60. Pimenta, A.F., Zhukareva, V., Barbe, M.F., Reinoso, B.S., Grimley, C., Henzel, W., Fischer, I., and Levitt, P. (1995). The limbic system-associated membrane protein is an Ig superfamily member that mediates selective neuronal growth and axon targeting. Neuron *15*, 287–297. https://doi.org/10.1016/0896-6273(95)90034-9.

61. Bontekoe, C.J.M., McIlwain, K.L., Nieuwenhuizen, I.M., Yuva-Paylor, L.A., Nellis, A., Willemsen, R., Fang, Z., Kirkpatrick, L., Bakker, C.E., McAninch, R., et al. (2002). Knockout mouse model for *Fxr2*: a model for mental retardation. Hum. Mol. Genet. *11*, 487–498. https://doi.org/10.1093/hmg/11.5.487.

62. Huynh, D.P., Maalouf, M., Silva, A.J., Schweizer, F.E., and Pulst, S.M. (2009). Dissociated fear and spatial learning in mice with deficiency of ataxin-2. PLoS One *4*, e6235. https://doi.org/10.1371/journal.pone.0006235.

63. Weskamp, K., Tank, E.M., Miguez, R., McBride, J.P., Gómez, N.B., White, M., Lin, Z., Gonzalez, C.M., Serio, A., Sreedharan, J., and Barmada, S.J. (2020). Shortened TDP43 isoforms upregulated by neuronal hyperactivity drive TDP43 pathology in ALS. J. Clin. Invest. *130*, 1139–1155. https://doi.org/10.1172/JCI130988.

64. Deshaies, J.E., Shkreta, L., Moszczynski, A.J., Sidibé, H., Semmler, S., Fouillen, A., Bennett, E.R., Bekenstein, U., Destroismaisons, L., Toutant, J., et al. (2018). TDP-43 regulates the alternative splicing of hnRNP A1 to yield an aggregation-prone variant in amyotrophic lateral sclerosis. Brain *141*, 1320–1333. https://doi.org/10.1093/brain/awy062.

65. Long, G., Chen, H., Wu, M., Li, Y., Gao, L., Huang, S., Zhang, Y., Jia, Z., and Xia, W. (2020). Antianemia drug roxadustat (FG-4592) protects against doxorubicin-induced cardiotoxicity by targeting antiapoptotic and antioxidative pathways. Front. Pharmacol. *11*, 1191. https://doi.org/10.3389/fphar.2020.01191.

66. Tamura, K., Stecher, G., and Kumar, S. (2021). MEGA11: molecular evolutionary genetics analysis version 11. Mol. Biol. Evol. *38*, 3022–3027. https://doi.org/10.1093/molbev/msab120.

67. Jones, D.T., and Cozzetto, D. (2015). DISOPRED3: precise disordered region predictions with annotated protein-binding activity. Bioinformatics *31*, 857–863. https://doi.org/10.1093/bioinformatics/btu744.

68. Xue, B., Dunbrack, R.L., Williams, R.W., Dunker, A.K., and Uversky, V.N. (2010). PONDR-FIT: a meta-predictor of intrinsically disordered amino acids. Biochim. Biophys. Acta *1804*, 996–1010. https://doi.org/10.1016/j.bbapap.2010.01.011.

69. Lancaster, A.K., Nutter-Upham, A., Lindquist, S., and King, O.D. (2014). PLAAC: a web and command-line application to identify proteins with prion-like amino acid composition. Bioinformatics *30*, 2501–2502. https://doi.org/10.1093/bioinformatics/btu310.

70. Davis, M.W., and Jorgensen, E.M. (2022). ApE, A plasmid editor: a freely available DNA manipulation and visualization program. Front. Bioinform. *2*, 818619. https://doi.org/10.3389/fbinf.2022.818619.

71. Schneider, C.A., Rasband, W.S., and Eliceiri, K.W. (2012). NIH Image to ImageJ: 25 years of image analysis. Nat. Methods *9*, 671–675. https://doi.org/10.1038/nmeth.2089.

72. Schindelin, J., Arganda-Carreras, I., Frise, E., Kaynig, V., Longair, M., Pietzsch, T., Preibisch, S., Rueden, C., Saalfeld, S., Schmid, B., et al. (2012). Fiji: an open-source platform for biological-image analysis. Nat. Methods *9*, 676–682. https://doi.org/10.1038/nmeth.2019.

73. Chen, S., Zhou, Y., Chen, Y., and Gu, J. (2018). fastp: an ultra-fast all-in-one FASTQ preprocessor. Bioinformatics *34*, i884–i890. https://doi.org/10.1093/bioinformatics/bty560.

74. Love, M.I., Huber, W., and Anders, S. (2014). Moderated estimation of fold change and dispersion for RNA-seq data with DESeq2. Genome Biol. *15*, 550. https://doi.org/10.1186/s13059-014-0550-8.

75. Sherman, B.T., Hao, M., Qiu, J., Jiao, X., Baseler, M.W., Lane, H.C., Imamichi, T., and Chang, W. (2022). DAVID: a web server for functional enrichment analysis and functional annotation of gene lists (2021 update). Nucleic Acids Res. *50*, W216–W221. https://doi.org/10.1093/nar/gkac194.

76. R Core Team (2020). R: A Language and Environment for Statistical Computing (R Foundation for Statistical Computing). https://www.R-project.org/.

77. Cunningham, F., Allen, J.E., Allen, J., Alvarez-Jarreta, J., Amode, M.R., Armean, I.M., Austine-Orimoloye, O., Azov, A.G., Barnes, I., Bennett, R., et al. (2022). Ensembl 2022. Nucleic Acids Res. *50*, D988–D995. https://doi.org/10.1093/nar/gkab1049.

78. Letunic, I., Khedkar, S., and Bork, P. (2021). SMART: recent updates, new developments and status in 2020. Nucleic Acids Res. *49*, D458–D460. https://doi.org/10.1093/nar/gkaa937.

79. Isobe, M., Toya, H., Mito, M., Chiba, T., Asahara, H., Hirose, T., and Nakagawa, S. (2020). Forced isoform switching of Neat1_1 to Neat1_2 leads to the loss of Neat1_1 and the hyperformation of paraspeckles but does not affect the development and growth of mice. RNA *26*, 251–264. https://doi.org/10.1261/rna.072587.119.

80. McGlincy, N.J., and Ingolia, N.T. (2017). Transcriptome-wide measurement of translation by ribosome profiling. Methods *126*, 112–129. https://doi.org/10.1016/j.ymeth.2017.05.028.

81. Takao, K., and Miyakawa, T. (2006). Light/dark transition test for mice. J. Vis. Exp. *1*, 104. https://doi.org/10.3791/104.

82. Shoji, H., Takao, K., Hattori, S., and Miyakawa, T. (2014). Contextual and cued fear conditioning test using a video analyzing system in mice. J. Vis. Exp. *85*, 50871. https://doi.org/10.3791/50871.

83. Komada, M., Takao, K., and Miyakawa, T. (2008). Elevated plus maze for mice. J. Vis. Exp. *22*, 1088. https://doi.org/10.3791/1088.

84. Porsolt, R.D., Bertin, A., and Jalfre, M. (1977). Behavioral despair in mice: a primary screening test for antidepressants. Arch. Int. Pharmacodyn. Ther. *229*, 327–336.

85. Matsuo, N., Takao, K., Nakanishi, K., Yamasaki, N., Tanda, K., and Miyakawa, T. (2010). Behavioral profiles of three C57BL/6 substrains. Front. Behav. Neurosci. *4*, 29. https://doi.org/10.3389/fnbeh.2010.00029.

86. Shoji, H., Takao, K., Hattori, S., and Miyakawa, T. (2016). Age-related changes in behavior in C57BL/6J mice from young adulthood to middle age. Mol. Brain *9*, 11. https://doi.org/10.1186/s13041-016-0191-9.

87. Moy, S.S., Nadler, J.J., Perez, A., Barbaro, R.P., Johns, J.M., Magnuson, T.R., Piven, J., and Crawley, J.N. (2004). Sociability and preference for social novelty in five inbred strains: an approach to assess autistic-like behavior in mice. Gene Brain Behav. *3*, 287–302. https://doi.org/10.1111/j.1601-1848.2004.00076.x.

88. Fujii, K., Koshidaka, Y., Adachi, M., and Takao, K. (2019). Effects of chronic fentanyl administration on behavioral characteristics of mice. Neuropsychopharmacol. Rep. *39*, 17–35. https://doi.org/10.1002/npr2.12040.

89. Shoji, H., Hagihara, H., Takao, K., Hattori, S., and Miyakawa, T. (2012). T-maze forced alternation and left-right discrimination tasks for assessing working and reference memory in mice. J. Vis. Exp. *26*, 3300. https://doi.org/10.3791/3300.

90. Nakayama, K., Ohashi, R., Shinoda, Y., Yamazaki, M., Abe, M., Fujikawa, A., Shigenobu, S., Futatsugi, A., Noda, M., Mikoshiba, K., et al. (2017). RNG105/caprin1, an RNA granule protein for dendritic mRNA localization, is essential for long-term memory formation. Elife *6*, e29677. https://doi.org/10.7554/eLife.29677.

STAR★METHODS

KEY RESOURCES TABLE

REAGENT or RESOURCE	SOURCE	IDENTIFIER
Antibodies		
Rabbit monoclonal anti-ILF3	Abcam	Cat#ab92355; RRID: AB_2049804
Rabbit polyclonal anti-ILF3	Proteintech	Cat#19887-1-AP; RRID: AB_10666431
Rabbit polyclonal anti-TDP-43	Proteintech	Cat#10782-2-AP; RRID: AB_615042
Rabbit polyclonal anti-hnRNPA1	Cell Signaling Technology	Cat#8443; RRID: AB_10828725
Rabbit polyclonal anti-α-tubulin	MBL International	Cat#PM054; RRID: AB_10598496
Rabbit monoclonal anti-c-Fos	Cell Signaling Technology	Cat#2250; RRID: AB_2247211
Rabbit polyclonal anti-MAP2	Abcam	Cat# ab32454; RRID: AB_776174
Mouse monoclonal anti-Tau-1	Sigma-Aldrich	MAB3420; PRID: AB_94855
Biotin-conjugated anti-rabbit Ig	Cytiva	Cat#RPN1004-2ML; RRID: AB_1062582
Alexa488-conjugated anti-rabbit IgG	Thermo Fisher Scientific	Cat#A-11034; RRID:AB_2576217
Cy3-conjugated anti-mouse IgG	Jackson ImmunoResearch	Code: 715-165-150; PRID: AB_2340813
Chemicals, peptides, and recombinant proteins		
Alkaline phosphatase-conjugated streptavidin	Cytiva	Cat#RPN12234
Turbo DNase	Thermo Fisher Scientific	Cat#AM2238
Opti-MEM1	Thermo Fisher Scientific	Cat#31985070
Cas9 protein	Integrated DNA Technologies	Cat#1081058
M2 medium	Sigma-Aldrich	Cat#MR-015-D
Penicillin-Streptomycin	Thermo Fisher Scientific	Cat#15140122
ISOGEN	Nippon Gene	Code: 311-02501
M-MLV-Reverse Transcriptase	Thermo Fisher Scientific	Cat#28025013
TB Green Premix Ex Taq II (Tli RNaseH Plus)	Takara Bio	Code: RR820A
Tissue-Tek O.C.T. Compound	Sakura Finetek	Code: 45833
4′,6-diamidino-2-phenylindole (DAPI)	FUJIFILM Wako Pure Chemical	Code: 340–7971
Mowiol 4-88	Sigma-Aldrich	Cat#81381
Neurobasal-A medium	Thermo Fisher Scientific	Cat#10888022
B-27 supplement	Thermo Fisher Scientific	Cat#17504044
L-Glutamine	Thermo Fisher Scientific	Cat#21051024
Neuron Culture Medium	FUJIFILM Wako Pure Chemical	Code: 148-09671
Formaldehyde	FUJIFILM Wako Pure Chemical	Code: 064-00406
TRIzol reagent	Thermo Fisher Scientific	Cat#10296010
RNase I	Lucigen	Code: N6901K
SUPERase In	Thermo Fisher Scientific	Cat#AM2694
ProtoScriptII	New England Biolabs	Cat#M0368L
CircLigase II	Lucigen	Code: CL9021K
Critical commercial assays		
mMESSAGE mMACHINE T7 Transcription Kit	Thermo Fisher Scientific	Cat#AM1344
MEGAclea Transcription Clean-Up Kit	Thermo Fisher Scientific	Cat#AM1908
ExoSAP-IT	Thermo Fisher Scientific	Cat#78201.1.ML
MEGAshortscript T7 Transcription Kit	Thermo Fisher Scientific	Cat#AM1354
Qubit RNA HS Assay Kit	Thermo Fisher Scientific	Cat#Q32852

(*Continued on next page*)

Continued

REAGENT or RESOURCE	SOURCE	IDENTIFIER
Ribo-Zero Gold rRNA Removal Kit Human/Mouse/Rat)	Illumina	Cat#MRZG12324
TruSeq Stranded mRNA Library Prep Kit	Illumina	Cat#20020595
Direct-zol RNA MicroPrep Kit	Zymo Research	Cat#R2060
Deposited data		
RNA-seq and ribosome profiling data	This paper	GEO: GSE209902
Experimental models: Organisms/strains		
Mouse: *Ilf3*$^{+/\Delta PrLD}$	This paper	N/A
Mouse: *Ilf3*$^{+/-}$	This paper	N/A
Oligonucleotides		
CRISPR/Cas9 targeting sequence: ILF3 ΔPrLD: CCCTGTCTAGGTCAGTTCTACAG	This paper	N/A
ssODN: ILF3 ΔPrLD: CGGCTGCG GGCCAGCCTTCAGGGCCCATGACTG CTCCTTCCTCCCCTCCCAGCCCTC ACCCTGGGACCATCCATCTAATC TGCTGCTTCCCTGTCTAGGT TAGTTCTACAGCAATGGAGG GCATTCTGGGAATGCCGGT GGTGGAGGCAGCGGGGGA GGTGGTGGCTCATCCAGCT ACAGCTCCTACTACCAAGGAGACA	This paper	N/A
Primer: ILF3 ΔPrLD genotyping Forward: ATCAGCTGAGGGTGAGTGGAGCTG	This paper	N/A
Primer: ILF3 ΔPrLD genotyping Reverse: TGCAGCGGCTTCTTCCCAGCATGC	This paper	N/A
CRISPR/Cas9 targeting sequence: ΔILF3: CGTCCCTCCGACACGCCAAG	This paper	N/A
Primer: ΔILF3 screening Forward: GAGCTGATGGCACTTTAGCC	This paper	N/A
Primer: ΔILF3 screening Reverse: AGTCTCCTCAGGGCTGTCAA	This paper	N/A
Primer: ΔILF3 genotyping Forward: TTCTGTGGTTTAAATTTGGGAGAGG	This paper	N/A
Primer: ΔILF3 genotyping Reverse control: AAAATGCAAACCTGGAACCACTTG	This paper	N/A
Primer: ΔILF3 genotyping Reverse: AAATGCAAACCTTGGCGGAG	This paper	N/A
Primer: NFARs qRT-PCR Forward: AGACAGGCCCTGTTCATGCT	This paper	N/A
Primer: NFARs qRT-PCR Reverse: TTGGCAAGCCCATGTCCTGT	This paper	N/A
Primer: NFAR2 qRT-PCR Forward: ACGCTTTGAGGTGTGGTGGT	This paper	N/A
Primer: NFAR2 qRT-PCR Reverse: AACGGCAAGACCTCGGAACA	This paper	N/A
Primer: NFAR1 qRT-PCR Forward: TCTACACTGCCTGGCACACA	This paper	N/A

(*Continued on next page*)

Continued

REAGENT or RESOURCE	SOURCE	IDENTIFIER
Primer: NFAR1 qRT-PCR Reverse: AGGGGCAGTTCTGCAGCAAA	This paper	N/A
Primer: GAPDH qRT-PCR Forward: AACGACCCCTTCATTGACCT	This paper	N/A
Primer: GAPDH qRT-PCR Reverse: TGGAAGATGGTGATGGGCTT	This paper	N/A
Primer: Hba-a1 qRT-PCR Forward: CGATGCTCTGGCCAATGCTG	This paper	N/A
Primer: Hba-a1 qRT-PCR Reverse: GCTAGCCAAGGTCACCAGCA	This paper	N/A
Primer: mt-Atp8 qRT-PCR Forward: ACATTCCCACTGGCACC	Long et al.[65]	N/A
Primer: mt-Atp8 qRT-PCR Forward: GGGGTAATGAATGAGGC	Long et al.[65]	N/A
Primer: mt-Nd3 qRT-PCR Forward: GCATTCTGACTCCCCCAAAT	Weger et al.[43]	N/A
Primer: mt-Nd3 qRT-PCR Reverse: TGAATTGCTCATGGTAGTGGA	Weger et al.[43]	N/A
Primer: mt-Nd6 qRT-PCR Forward: GTATTGGGGGTGATTATAGAG	This paper	N/A
Primer: mt-Nd6 qRT-PCR Reverse: CCATCATTCAAGTAGCACAAC	This paper	N/A
Primer: Tubb5 qRT-PCR Forward: ACTATGGACTCCGTTCGCTCAG	This paper	N/A
Primer: Tubb5 qRT-PCR Reverse: ACAGAGTCAACCAACTCAGCTCC	This paper	N/A
Primer: Sgk1 qRT-PCR Forward: GGTGCCAAGGATGACTTTATGGA	This paper	N/A
Primer: Sgk1 qRT-PCR Reverse: GGTAAACTCGGGATCGAAGTGC	This paper	N/A
Software and algorithms		
MEGA11	Tamura et al.[66]	https://www.megasoftware.net
DISOPRED3	Jones and Cozzetto[67]	http://bioinf.cs.ucl.ac.uk/psipred/
PONDR-FIT	Xue et al.[68]	http://original.disprot.org/pondr-fit.php
PLAAC	Lancaster et al.[69]	http://plaac.wi.mit.edu
ApE	Davis and Jorgensen[70]	https://jorgensen.biology.utah.edu/wayned/ape/
ImageJ	Schneider et al.[71]	https://imagej.nih.gov/ij/
Fiji	Schindelin et al.[72]	https://fiji.sc
fastp	Chen et al.[73]	https://github.com/OpenGene/fastp
DESeq2 package	Love et al.[74]	https://bioconductor.org/packages/release/bioc/html/DESeq2.html
DAVID Bioinformatics Resources	Sherman et al.[75]	https://david.ncifcrf.gov/home.jsp
R	R Core Team[76]	https://www.r-project.org
Other		
Raw data of behavioral test battery	This paper	http://www.mouse-phenotype.org/

RESOURCE AVAILABILITY

Lead contact

Further information and requests for resources and reagents should be directed to and will be fulfilled by the lead contact, Nobuyuki Shiina (nshiina@nibb.ac.jp).

Material availability

Mouse lines generated in this study are available from the lead contact with a completed Material Transfer Agreement.

Data and code availability

- The RNA-Seq and ribosome profiling data used in this study have been deposited at GEO and are publicly available as of the date of publication. The accession number is listed in the key resources table. The raw data of behavioral test battery are disclosed in the gene-brain-phenotyping database (http://www.mouse-phenotype.org/), as listed in the key resources table. All data reported in this paper will be shared by the lead contact upon request.
- This paper does not report original code.
- Any additional information required to reanalyze the data reported in this paper is available from the lead contact upon request.

EXPERIMENTAL MODEL AND SUBJECT DETAILS

Mice

Mice were maintained on a C57BL/6J genetic background. All animal care and experiments were approved by the Animal Experiment Committee of the National Institutes of Natural Sciences and the University of Toyama and performed in accordance with the guidelines from the National Institutes of Natural Sciences, University of Toyama, and Science Council of Japan.

METHOD DETAILS

Phylogenetic analysis of DZF-containing proteins

Amino acid sequences of DZF-containing proteins were obtained from Ensemble[77] and SMART.[78] The phylogenetic tree was constructed by the maximum likelihood algorithm using MEGA11.[66]

IDR and PrLD predictions

IDR predictions were performed using the DISOPRED3[67] and PONDR-FIT[68] predictors. PrLD predictions were conducted with the PLAAC predictor.[69]

Generation of ILF3 PrLD-deficient mice

ILF3 PrLD-deficient mice were generated following procedures described previously.[79] Briefly, gRNA, which targets the exon 20 sequence 5′-CCCTGTCTAGGTCAGTTCTACAG-3′ of the *Ilf3* gene, and Cas9 mRNA were transcribed *in vitro* using the mMESSAGE mMACHINE T7 Transcription Kit (Thermo Fisher Scientific, Waltham, MA), and purified with the MEGAclear Transcription Clean-Up Kit (Thermo Fisher Scientific). Single-stranded oligo-DNA (ssODN) was synthesized to introduce a stop codon at the 5′ most region of the ILF3 PrLD coding exon. The sequence of ssODN was 5′-CGGCTGCGGGCCAGCCTTCAGGGCCCATGACTGCTCCTTCCTCCCCTCCCAGCCCTCACCCTGGGACCATCCATCTAATCTGCTGCTTCCCTGTCTAGGTTAGTTCTACAGCAATGGAGGGCATTCTGGGAATGCCGGTGGTGGAGGCAGCGGGGGAGGTGGTGGCTCATCCAGCTACAGCTCCTACTACCAAGGAGACA-3′. The RNA and DNA were mixed at concentrations of 25 ng/μl Cas9 mRNA, 12.5 ng/μl gRNA, and 100 ng/μl ssODN, and the injection into fertilized eggs was performed at the RIKEN Research Resource Center.

For genotyping of the ILF3 PrLD-deficient mice, the *Ilf3* genomic region containing the substituted nucleotide was amplified using primers 5′-ATCAGCTGAGGGTGAGTGGAGCTG-3′ and 5′-TGCAGCGGCTTCTTCCCAGCATGC-3′ (PrLD-R). The 1 μl PCR products were diluted with 11.3 μl water and treated with 0.2 μl ExoSAP-IT (Thermo Fisher Scientific) to remove the primers. The purified PCR products were sequenced using the PrLD-R primer. To confirm the single nucleotide substitution in the *Ilf3* gene, DNA sequencing chromatograms were visualized with ApE software.[70]

Generation of ILF3 deficient mice

The ILF3 deficient mice were generated using a CRISPR/Cas9 system with modifications to previous studies.[47] The gRNA was generated to target the exon 7 sequence 5′-CGTCCCTCCGACACGCCAAG-3′ of the *Ilf3* gene. The gRNA template DNA containing the T7 promoter, gRNA spacer (the target sequence), and gRNA scaffold was synthesized using the gBlocks gene fragments service (Integrated DNA Technologies, Coralville, IA) and transcribed to gRNA using the MEGAshortscript T7 Transcription Kit (Thermo Fisher Scientific). The synthesized gRNA was treated with 0.3 U/μl Turbo DNase (Thermo Fisher Scientific) at 37°C for 15 min, purified using phenol-chloroform extraction and ethanol precipitation, and dissolved in Opti-MEM1 (Thermo Fisher Scientific).

In vitro fertilized eggs from C57BL/6J strain mice were washed three times with modified Whitten's medium (mWM) 4 hours after fertilization and then aligned in an electrode gap, which was filled with opti-MEM1 containing 200 ng/μl Cas9 protein (Integrated DNA Technologies) and 200 ng/μl gRNA. Electroporation was performed using a Genome Editor (BEX Co. Ltd., Tokyo, Japan) at 25 V (3 msec ON + 97 msec OFF) three times, alternating the current direction. After electroporation, the eggs were washed three times with M2 medium (Sigma-Aldrich, Burlington, MA) containing 100 units/ml Penicillin-Streptomycin (Thermo Fisher Scientific) and cultured overnight in mWM. On the next day, the surviving 2-cell stage zygotes were transferred to the oviducts of pseudopregnant females.

To identify mutations in the *Ilf3* gene that were generated by CRISPR/Cas9, the genomic region containing the gRNA target was amplified by PCR using primers 5′-GAGCTGATGGCACTTTAGCC-3′ (exon7-F) and 5′-AGTCTCCTCAGGGCTGTCAA-3′. The 1 μl PCR products were diluted with 11.3 μl water and treated with 0.2 μl ExoSAP-IT (Thermo Fisher Scientific) to remove the primers. The purified PCR products were sequenced using the exon7-F primer. To confirm the insertions and deletions of nucleotides, DNA sequencing chromatograms were visualized using ApE software. Genotyping of the $Ilf3^{+/-}$ mice, which have the $Ilf3^{-}$ allele with 14-bp deletion, was performed by PCR using primers 5′-TTCTGTGGTTTAAATTT GGGAGAGG-3′ (common forward primer) and 5′-AAAATGCAAACCTGGAACCACTTG-3′ to detect the $Ilf3^{+}$ allele, and the common forward primer and 5′-AAATGCAAACCTTGGCGGAG-3′ to detect the $Ilf3^{-}$ allele.

Water-immersion and restraint stress (WIRS)

Mice were housed in home cages in pairs of identical genotypes (1 or 2 pairs/cage) with a 12-hour light/dark cycle. The mice in the stress group were placed in a 50 mL conical polypropylene centrifuge tube with holes for breathing and soaked in water to a level where the nose was not submerged for 3 hours a day during the light cycle over 14 days. Mice were weighed daily just prior to WIRS (see Figures S11A–S11C). The mice in the control group, which were placed in a home cage separate from the stress group to avoid the effects of interactions between the stressed and control individuals, remained in the home cage during the stress exposure period.

Quantification of mRNA expression

Total RNA was extracted from mouse tissues using ISOGEN (Nippon Gene, Tokyo, Japan) according to the manufacturer's protocol. Reverse transcription (RT) was performed with M-MLV-Reverse Transcriptase (Thermo Fisher Scientific) and quantitative PCR was performed with TB Green Premix Ex Taq II (Tli RNaseH Plus) (Takara Bio, Shiga, Japan) according to the manufacturer's protocols using the 7500 real-time PCR system (Thermo Fisher Scientific). The expression level of each gene was quantified by a standard curve method using the same gene as a standard. The primers used for quantitative RT-PCR were: 5′-AGACA GGCCCTGTTCATGCT-3′ and 5′-TTGGCAAGCCCATGTCCTGT-3′ for NFARs (both NFAR1 and NFAR2); 5′-ACGCTTTGAGGTGTGGTGGT-3′ and 5′-AACGGCAAGACCTCGGAACA-3′ for NFAR2; 5′-TCTACAC TGCCTGGCACACA-3′ and 5′-AGGGGCAGTTCTGCAGCAAA-3′ for NFAR1; 5′-AACGACCCCTTCATTGA CCT-3′ and 5′-TGGAAGATGGTGATGGGCTT-3′ for GAPDH; 5′-CGATGCTCTGGCCAATGCTG-3′ and 5′-GCTAGCCAAGGTCACCAGCA-3′ for Hba-a1; 5′-ACATTCCCACTGGCACC-3′ and 5′-GGGGTAATGA ATGAGGC-3′ for mt-Atp8; 5′-GCATTCTGACTCCCCCAAAT-3′ and 5′-TGAATTGCTCATGGTAGTGGA-3′ for mt-Nd3; 5′-GTATTGGGGGTGATTATAGAG-3′ and 5′-CCATCATTCAAGTAGCACAAC-3′ for mt-Nd6; 5′-ACTATGGACTCCGTTCGCTCAG-3′ and 5′-ACAGAGTCAACCAACTCAGCTCC-3′ for Tubb5; and 5′-GGTGCCAAGGATGACTTTATGGA-3′ and 5′-GGTAAACTCGGGATCGAAGTGC-3′ for Sgk1.

Western blotting

Mouse tissue extracts were prepared by homogenization and sonication in Laemmli sample buffer. After boiling for 5 min, the extracts were loaded onto SDS-polyacrylamide gels and transferred to polyvinylidene difluoride membranes (Merck KGaA, Darmstadt, Germany). The membranes were probed with anti-ILF3 rabbit monoclonal antibody (ab92355, Abcam, Cambridge, UK), anti-ILF3 rabbit polyclonal antibody (19887-1-AP, Proteintech, Chicago, IL), and anti-α-tubulin rabbit polyclonal antibody (PM054, Medical & Biological Laboratories, Nagoya, Japan). Biotinylated secondary antibody (Cytiva, Marlborough, MA) and alkaline phosphatase-conjugated streptavidin (Cytiva) were used for the detection of protein bands in a bromochloroindolyl phosphate/nitro blue tetrazolium solution. Quantitative comparisons of band intensities between the genotypes were performed as previously described using standard curves generated from the dilution series of each tissue extract from the *Ilf3*$^{+/+}$ mice on the same membrane.[49] The NFAR2/NFAR1 band intensity ratio was calculated by measuring the NFAR1 and NFAR2 bands in the same lane using ImageJ software.[71]

Immunostaining

The brains of adult mice were embedded in Tissue-Tek O.C.T. Compound (Sakura Finetek, Tokyo, Japan), frozen in liquid nitrogen, and sliced to a thickness of 12 μm for ILF3 staining and 30 μm for c-Fos staining using a cryostat (Leica CM1950, Leica, Wetzlar, Germany). The sections were mounted on silane-coated coverslips and dried at room temperature. The samples were fixed in 3.7% formaldehyde in phosphate-buffered saline (PBS) for 10 min, washed with PBS, and treated with blocking buffer (10% fetal bovine serum (FBS) and 0.1% Triton X-100 in PBS) for 1 h at room temperature. The samples were then incubated with primary antibodies in blocking buffer at 4°C overnight. The primary antibodies used were the anti-ILF3 rabbit monoclonal antibody (Abcam), anti-TDP-43 rabbit polyclonal antibody (10782-2-AP, Proteintech, Rosemont, IL, USA), anti-hnRNPA1 rabbit monoclonal antibody (#8443, Cell Signaling Technology, Danvers, MA), and anti-c-Fos rabbit monoclonal antibody (#2250, Cell Signaling Technology). After washing with PBS, the samples were stained with Alexa488-conjugated anti-rabbit IgG antibody (Thermo Fisher Scientific) and 4′,6-diamidino-2-phenylindole (DAPI) (FUJIFILM Wako Pure Chemical, Osaka, Japan) in blocking buffer at 4°C overnight. The samples were washed with PBS and mounted in Mowiol (Sigma-Aldrich). Fluorescence images were acquired using an A1 confocal laser scanning microscope equipped with a Ti-E inverted microscope (Nikon, Tokyo, Japan) and a 20× or 60× objective.

The fluorescence images were analyzed using ImageJ/Fiji software.[72] To calculate the nuclear-cytoplasmic ratio of staining intensity, the images were processed by background subtraction and mean-filtering. The fluorescence intensity of the whole cells and nuclei was measured using the ROI manager, and the intensity of the cytoplasm was calculated by subtracting the intensity of nuclei from the intensity of whole cells. The nuclear-cytoplasmic ratio was calculated by dividing the mean intensity per pixel in the nucleus by that in the cytoplasm. To count the number of c-Fos positive cells, the images were z-stacked (all consecutive images acquired in 1 μm steps) and binarized using the "Triangle" auto threshold function. Particles (c-Fos-positive cells) with a size of 30-200 pixels were counted using the "Analyze particles" function. Multiple cells that were counted as one because they overlapped on the image were manually recounted. Particles that did not overlap with DAPI-stained nuclei were not counted.

Quantification of NFARs-containing granules in the nucleus

Mice were perfused with PBS and subsequently with 3.7% formaldehyde in PBS for fixation using a peristaltic pump (MP-2000, Tokyo Rikakikai, Tokyo, Japan). The brain was removed and post-fixed with 3.7% formaldehyde in PBS overnight at 4°C. The brain was coronally sectioned at a thickness of 50 μm using a vibratome (VT1200S, Leica, Germany). Immunostaining was performed as described above. Fluorescence images were acquired consecutively in 1 μm steps using the A1 confocal laser scanning microscope with a 60× objective. The number and size of NFARs-containing granules in the nucleus were quantified using ImageJ/Fiji software. The quantification used 5 consecutive images with the maximum diameter of the nucleus. Granules that overlapped when the consecutive images were stacked were judged to be the same granule. Granule size was measured in one of the consecutive images with the largest diameter of the overlapping granules.

Analysis of neurite formation in cultured AMY neurons

Dissociated AMY neurons were prepared from *Ilf3*$^{+/+}$ and *Ilf3*$^{\Delta PrLD/\Delta PrLD}$ littermates at embryonic day 16-18 (E16-18). Neurons were plated at a density of 5.2 × 10^3 cells/cm^2 onto poly-D-lysine-coated coverslips (Matsunami, Osaka, Japan) in Neurobasal-A medium (Thermo Fisher Scientific) containing B-27 supplement (Thermo Fisher Scientific), 0.5 mM glutamine, and 25% Neuron culture medium (FUJIFILM Wako Pure Chemical). Cultured neurons were incubated at 37°C in a 5% CO_2 incubator. They were fixed with 3.7% formaldehyde in PBS for 10 min at 3, 5, and 7 days *in vitro* (DIV).

Immunostaining was performed as described above. The primary antibodies used were anti-MAP2 rabbit polyclonal antibody (ab32454, Abcam) and anti-Tau-1 mouse monoclonal antibody (MAB3420, Sigma-Aldrich). Secondary antibodies were Alexa488-conjugated anti-rabbit IgG antibody (Thermo Fisher Scientific) and Cy3-conjugated anti-mouse IgG antibody (Jackson ImmunoResearch, West Grove, PA). Fluorescence images were acquired using the A1 confocal laser scanning microscope with a 20× or 40× objective. Serial images acquired at 0.5 μm steps were z-stacked. Concentric circles were drawn at 30 μm intervals around the nucleus for Sholl analysis, where the number of intersections was counted. One of the neurites with the strongest tau staining was determined to be the axon.

RNA-seq and ribosome profiling

The *Ilf3*$^{+/+}$ and *Ilf3*$^{\Delta PrLD/\Delta PrLD}$ mice in the stress group were exposed to WIRS for 3 h a day for 14 days. The amygdala of control mice without WIRS and stressed mice with WIRS were isolated from the brains and quickly frozen in liquid nitrogen. The samples were lysed in ice-cold lysis buffer (20 mM Tris-HCl, pH 7.5, 150 mM NaCl, 5 mM $MgCl_2$, 1 mM DTT, 100 μg/ml cycloheximide, 100 μg/ml chloramphenicol, and 1% Triton X-100) using a beads shocker (Yasui Kikai, Osaka, Japan), treated with 25 U/ml Turbo DNase (Thermo Fisher Scientific) on ice for 10 min, and centrifuged at 20,000 g for 10 min at 4°C. The RNA concentration of lysate was measured using a Qubit RNA HS Assay Kit (Thermo Fisher Scientific). The lysate was split into two for the use in RNA-seq and ribosome profiling.

For RNA-seq analysis, the total RNA was extracted using TRIzol reagent (Thermo Fisher Scientific) from the lysate containing 500 ng RNA. The rRNA was removed using the Ribo-Zero Gold rRNA Removal Kit (Human/Mouse/Rat) (Illumina, San Diego, CA). The cDNA libraries were prepared using the TruSeq Stranded mRNA Library Prep Kit (Illumina).

Ribosome profiling was conducted as previously reported[46,80] with modifications. Lysate containing 1.5 μg RNA was treated with 3 U of RNase I (Lucigen, Middleton, WI) at 25°C for 45 min, followed by the addition of 10 μl SUPERase In (Thermo Fisher Scientific) to stop nuclease digestion. The sample was overlaid on a 1 M sucrose cushion and the ribosomes were pelleted by centrifugation for 1 h at 100,000 rpm at 4°C in a TLA-110 rotor (Beckman Coulter, Brea, CA). Ribosome-bound RNA was isolated using a Direct-zol RNA MicroPrep Kit (Zymo Research, Irvine, CA). After gel electrophoresis, RNA fragments corresponding to 17-34 nt were excised. After ligating the RNA fragments to preadenylated linkers, ribosomal RNAs were removed with a Ribo-Zero Gold rRNA Removal Kit (Human/Mouse/Rat) (Illumina). Reverse transcription was performed by incubation with ProtoScriptII (New England Biolabs, Ipswich, MA) at 50°C for 30 min. The cDNAs were circularized by CircLigase II (Lucigen) and PCR-amplified.

The libraries for RNA-seq and ribosome profiling were sequenced on a HiSeq4000 (Illumina). Read quality filtering and adapter trimming were conducted using fastp.[73] After removing noncoding RNA-mapped reads, the remaining reads were aligned to the mouse genome of GRCm38/mm10. For ribosome profiling, the A-site offsets from the 5′ end were determined to be 15 for 28-31 nt and 16 for 32-33 nt for cyto-ribosome footprints in the *Ilf3*$^{+/+}$ and *Ilf3*$^{\Delta PrLD/\Delta PrLD}$ mice; 14 for 21- 28 nt, 15 for 29-33 nt, and 16 for 34 nt for mito-ribosome footprints in the *Ilf3*$^{+/+}$ mice; 13 for 22 nt, 14 for 21, 23-29, and 31 nt, and 15 for 30 and 32-34 nt for mito-ribosome footprints in the *Ilf3*$^{\Delta PrLD/\Delta PrLD}$ mice. For RNA-seq, an offset of 15 was used for all mRNA fragments. We used the GENCODE VM23 gene annotation and transcripts. The differential expression analysis of RNA-seq and ribosome profiling was performed using the DESeq2 package.[74] Translation efficiency, which is the number of reads in ribosome profiling normalized by that in RNA-seq, was also analyzed using DESeq2. Significance was calculated using the likelihood ratio test in a generalized linear model. Reads corresponding to the first and the last 5 codons in the coding sequence were excluded from the analysis. Two replicates from 4 mice were analyzed in each group (each replicate consists of samples from two mice).

Gene ontology enrichment analysis

GO enrichment analysis was performed using the DAVID Bioinformatics Resources.[75] The annotation categories used were GOTERM_BP_DIRECT and KEGG_PATHWAY. The significance of the overrepresentation of GO terms was assessed using the Benjamini-Hochberg false discovery rate (FDR) criterion at $p < 0.05$.

Design of comprehensive behavioral test battery

Male *Ilf3*$^{+/+}$ and *Ilf3*$^{\Delta PrLD/\Delta PrLD}$ littermates were group-housed (2 pairs/cage) in a room with a 12-hour light/dark cycle. All mice had access to food and water *ad libitum*. A battery of behavioral tests was conducted in the following sequence starting at 11 weeks of age (Table 1): general health and neurologic screening (body weight, body temperature, grip strength, and wire hang), light/dark transition, open field, elevated plus maze, hot plate, social interaction test, rotarod test, three-chamber social approach test (100 lux), startle response and prepulse inhibition, Porsolt forced swim test, Barnes maze, T-maze (spontaneous alternation), contextual and cued fear conditioning test, three-chamber social approach test (5 lux), social interaction test in a home cage, and tail suspension test. All testing apparatuses were cleaned with diluted hypochlorous solution or 70% ethanol for each test to prevent biases due to olfactory cues.

Body weight and body temperature

Body weight was measured using a weight scale with the mice placed in a stainless bowl. For body temperature, the rectal temperature was measured.

Open field test

Mice were placed in an open field apparatus (40 × 40 × 30 cm; AccuScan Instruments, Columbus, OH) illuminated at 100 lux. The total distance traveled, vertical activity (rearing measured by counting the number of photobeam interruptions), and time spent in the center area of the field were recorded for 120 min using the VeraMax system (AccuScan Instruments).

Light/dark transition test

The light/dark transition test was conducted as previously described.[81] Mice were placed in a dark chamber and the door was opened 3 seconds later. The mice were free to move between the two chambers for 10 min with the door open. The total number of transitions between chambers, latency to the first entry to the light chamber, the time spent in each chamber, and the total distance traveled were recorded automatically using the ImageLD program (see section, "Data analysis in behavioral test battery").

Barnes maze test

The Barnes maze test was conducted as previously described.[48] An escape box containing paper bedding was placed under the target hole. Mice were trained in 12 trials. 24 hours after the last training, a probe trial (PT1) was performed without the escape box. 1 month after PT1, another probe trial (PT2) was performed to evaluate memory retention (see Figure S8D). After PT2, mice were trained in 6 additional trials, in which the location of the target hole was not changed from the initial training trials. The mice then underwent a reversal training session. In the reversal training, the location of the target hole was changed to the opposite side of the maze, and the mice were trained in 6 trials. Then, 24 hours after the last reversal training, another probe trial (PT3) was performed (see Figure S8F). The data acquisition and analysis were performed automatically using ImageBM program (see section, "Data analysis in behavioral test battery").

Contextual and cued fear conditioning test

The contextual and cued fear conditioning test was conducted as previously described.[82] Mice were placed in a square test chamber with a metal grid floor. Then, 55 dB of white noise was presented as a conditioned stimulus (CS) for 30 seconds, and a 0.3 mA foot shock was given to the mice as an unconditioned stimulus (US) during the last 2 seconds of the white noise. Each mouse received three CS-US pairings at 2-min intervals in a conditioning session. Then, 24 hours after the conditioning session, a contextual test and a cued test with altered context were performed. In the contextual test, the mice were placed in the same test chamber as the conditioning session for 5 min without CS or US. In the cued test with altered context, the mice were placed in a novel triangular test chamber for 6 min. CS and US were not presented during the first 3 min, and only CS (55 dB white noise) was presented during the last 3 min. Freezing responses during

the conditioning, contextual testing, and cued testing sessions were measured automatically using the ImageFZ program (see section, "Data analysis in behavioral test battery").

Neuromuscular examination

Neuromuscular strength was examined by grip strength and wire hang tests. A grip strength meter (O'Hara & Co., Tokyo, Japan) was used to measure the mouse forelimb grip strength. Mice were held by the tail to allow their forelimbs to grip the wire grid. The mice were then gently pulled backward by the tail until they released the wire grid. The maximum force generated by the mouse forelimbs was recorded. Each mouse was tested three times and the greatest value was used for analysis. In the wire hang test, a box (22 × 22 × 30 cm) with a wire mesh grid (10 × 10 cm) on the top surface (O'Hara & Co.) was used. Mice were placed on the wire mesh grid, and it was inverted gently so that the mice gripped the wire. Latency to fall from the wire was recorded with a cutoff time of 60 sec.

Hot plate test

Mice were placed on a 55.0 ± 0.3°C hot plate (Columbus Instruments, Columbus, OH), and the latency to the first paw response was recorded. The paw response was defined as either paw shaking or licking.

Rotarod test

Motor coordination and balance were tested with the rotarod test. An accelerating rotarod (UGO Basile, Varese, Italy) was used. Mice were placed on a rotating rod (3 cm diameter), and the latency until the mice fell from the rod was measured. The speed of the rotarod accelerated from 4 to 40 rpm in 5 min.

Elevated plus maze test

The elevated plus maze test, which is widely used to assess anxiety-like behavior, was conducted as previously described.[83] The apparatus comprised two arms without walls (open arms, 25 × 5 cm), two arms of the same size with transparent walls (15 cm high) (closed arms), and a central square (5 × 5 cm) connecting the arms, which were at 90° to each other (O'Hara & Co., Tokyo, Japan). Arms of the same type were located opposite one another. The arms and the central square were elevated to a height of 55 cm above the floor. Mice were placed in the central square and allowed to freely explore the maze for 10 min. The number of arm entries, the percentage of entries into the open arms, the distance traveled, and the percentage of time spent in the open arms were measured automatically using the ImageEP program (see section, "Data analysis in behavioral test battery").

Porsolt forced swim test

The Porsolt forced swim test[84] was performed to assess depression-related behaviors. Mice were placed in a Plexiglas cylinder (20 cm height × 10 cm diameter, O'Hara & Co.), filled with water (23°C) up to 7.5 cm high, for 10 min a day for two consecutive days. The percentage of time spent immobile was measured automatically using the ImagePS program (see section, "Data analysis in behavioral test battery").

Tail suspension test

The tail suspension test was performed to assess depression-related behaviors. Mice were suspended by their tails with adhesive tape 30 cm above the floor of a chamber (31 × 41 × 41 cm) (O'Hara & Co.), and the percentage of time spent immobile during a 10-min test period was recorded using the ImageTS program (see section, "Data analysis in behavioral test battery").

Startle response/prepulse inhibition test

The startle response and prepulse inhibition test was conducted as previously described.[85] A startle reflex measurement system (O'Hara & Co.) was used. Mice were placed in a Plexiglas cylinder and left undisturbed for 10 min for habituation just before the test. In the test, 110 or 120 dB of white noise was used for 40 msec as a startle stimulus. The background noise level was 70 dB. The prepulse sound was presented 100 msec before the startle stimulus, and its intensity was 74 or 78 dB. The test session consisted of six consecutive trial types: two types of startle stimulus-only trials (110 and 120 dB) and four types of prepulse inhibition trials (74-110, 78-110, 74-120, and 78-120 dB). The average inter-trial interval was 15 sec (range 10-20 sec). The startle response was recorded for 140 msec, measuring the response every millisecond, starting with the onset of the prepulse stimulus. The peak startle amplitude recorded during the 140-msec sampling window was used as the dependent variable.

Social interaction test in a novel environment

Social interaction was measured in a novel environment as previously described.[86] Weight-matched (within 2 g) mice that had been housed in different cages were placed together in a box (40 × 40 × 30 cm) and allowed to explore freely for 10 min. The total number of contacts, total duration of contacts, mean duration per contact, and total distance traveled were measured automatically using the ImageSI program (see section, "Data analysis in behavioral test battery").

Three-chambered social approach test

The test for sociability and social novelty preference was conducted as previously described.[87,88] The apparatus comprised a rectangular, three-chambered box and a lid with a video camera (O'Hara & Co.), and was illuminated at 100 or 5 lux. Each chamber measured 20 × 40 × 47 cm, and the partition walls were made of clear Plexiglas with a small square opening (5 × 3 cm) allowing access to each chamber. First, the test mice were placed in the three-chambered box and allowed to explore for 10 min for habituation, during which an empty wire cage (9 cm in diameter, 11 cm in height, with vertical bars 0.5 cm apart) was placed in the outer corner of each of the left and right chambers. In the test session, an unfamiliar male mouse (stranger 1) that had no prior contact with the test mouse was placed in a wire cage in one of the side chambers. An empty wire cage was placed in the corner of the other side chamber. The location of the stranger mouse in the left vs right chamber was systematically alternated between trials. The test mice were placed in the central chamber and allowed to explore the entire box for 10 min to assess sociability (sociability test). In the next session, another unfamiliar male mouse (stranger 2) was placed in the wire cage that had been empty during the sociability test to evaluate social preference for a new stranger (social novelty preference test). Thus, the test mouse had a choice between the familiar mouse already investigated (stranger 1) and the novel unfamiliar mouse (stranger 2). The time spent around each cage was automatically calculated from video images using the ImageCSI program (see section, "Data analysis in behavioral test battery").

Social interaction test in a home cage

Monitoring of social behavior between two mice in a familiar environment was conducted as previously described.[48] Two mice of the same genotype, which had been housed separately, were placed together in a home cage. Their social interaction and locomotor activity were monitored for seven days. Social interaction was measured by counting the number of particles detected in each frame. In that measurement, two particles indicated that the two mice were separated from each other, and one particle indicated that they were in contact with each other. Data acquisition and analysis were performed automatically using ImageHCSI (see section, "Data analysis in behavioral test battery").

T-maze (spontaneous alternation)

The T-maze test was conducted as previously described[89] using an automated modified T-maze apparatus (O'Hara & Co.). Mice were allowed to freely run 10 laps in a session and subjected to 5 sessions in total. The correct response in each lap means that the mouse has chosen the opposite direction to the last lap. Data acquisition and analysis were performed automatically using ImageTM (see section, "Data analysis in behavioral test battery").

Data analysis in the behavioral test battery

The behavioral data were acquired automatically using applications (ImageLD, ImageBM, ImageFZ, ImageEP, ImagePS, ImageTS, ImageSI, ImageCSI, ImageHCSI, and ImageTM) based on the public domain NIH Image and ImageJ programs, and modified for each test by Tsuyoshi Miyakawa (O'Hara & Co.). Statistical analysis was conducted using Stat View (SAS Institute, Cary, NC). The data were analyzed using the Student's t-test, one-way ANOVA, or two-way repeated measures ANOVA. The values in the graph are presented as mean ± SEM. In the bar plots, individual values are represented by dot plots.

Morris water maze

The Morris water maze was conducted as previously described.[90] A transparent platform (6 cm in diameter) was hidden below the surface of the water in a round water tank with a diameter of 110 cm. The water was clouded with non-toxic white paint (Sakura Color Products, Osaka, Japan). Spatial cues (4 different plane figures) were displayed on the wall of the tank. Mice were placed in the pool and the escape latency to the platform was measured. If the mouse found the platform within a 2-min time limit, then the mouse was allowed to stay on the platform for 30 seconds. If not, then the mouse was guided to the platform before

staying on the platform for 30 seconds. The starting position was changed randomly, but the platform position was fixed. In the training session, mice were given 6 trials per day for 7 consecutive days.

The day after the last trial of the training session, the mice underwent a probe test. The platform was removed from the pool and the swimming path of the mouse was tracked for 1 min using a computer-based video tracking system called ANY-Maze (Stoeling, Wood Dale, IL). The time spent in the target quadrant, where the hidden platform had been placed, and in the other quadrants was measured. The data were analyzed in R[76] using three-way repeated measures ANOVA.

Contextual fear conditioning test (passive avoidance)

The passive avoidance test was conducted using the LDK-M chamber (Melquest, Toyama, Japan) equipped with the SCANET system (Melquest). The day before the training day, the mice were allowed to freely explore both the light and dark chambers for 10 min with the door open to habituate themselves to the test environment. On the day of the training, the mice were placed in the light chamber, and after the door was opened, the mice were allowed to freely explore the chambers for 10 min. The time spent in the dark chamber was measured in the first 5 min (Pre). Then, when the mouse entered the dark chamber, the door was closed and the mouse received a foot shock (1.5 mA, 2-second duration, 4 times with 1-min intervals). After the foot shock, the mice were returned to their home cage. 5 min, 1day, and 1 week after the foot shock, the mice were replaced into the light chamber, allowing them to freely explore the chambers for 5 min after the door opened. During these 5-min periods, the time spent in the dark chamber was measured. The data were analyzed in R using three-way repeated measures ANOVA. Simple effects were analyzed after interaction was significant in the three-way repeated measures ANOVA.

QUANTIFICATION AND STATISTICAL ANALYSIS

Sample numbers and experimental repeats are indicated in the figures and figure legends. Statistical significance was calculated using the log-rank test, three-way repeated measures ANOVA, two-way repeated measures ANOVA, two-way ANOVA, one-way ANOVA, simple effect analysis, Welch's t-test, Tukey-Kramer test, and Student's t-test with R. In the bar plots, individual values were represented as dot plots. In the behavioral tests, mice that died before the end of each experiment or had outlier data were excluded from the data analysis.